Research Paper

THEMED ISSUE: Mantle to Surface Dynamics during the Transition from Subduction to Collision to Tectonic Escape: Results from the Continental Dynamics–Central Anatolian Tectonics (CD-CAT) Project

GEOSPHERE

GEOSPHERE, v. 16, no. 2

https://doi.org/10.1130/GES02135.1

7 figures; 1 table; 1 set of supplemental files

CORRESPONDENCE: meijersmaud@gmail.com; gilles.brocard1@univ-grenoble-alpes.fr; dwhitney@umn.edu; andreas.mulch@senckenberg.de

CITATION: Meijers, M.J.M., Brocard, G.Y., Whitney, D.L., and Mulch, A., 2020, Paleoenvironmental conditions and drainage evolution of the central Anatolian lake system (Turkey) during late Miocene to Pliocene surface uplift: Geosphere, v. 16, no. 2, p. 490–509, https://doi.org/10.1130/GES02135.1.

Science Editor: Andrea Hampel
Guest Associate Editor: Susan L. Beck

Received 26 February 2019
Revision received 3 July 2019
Accepted 20 December 2019

Published online 10 January 2020

Paleoenvironmental conditions and drainage evolution of the central Anatolian lake system (Turkey) during late Miocene to Pliocene surface uplift

Maud J.M. Meijers[1,2], Gilles Y. Brocard[3,4], Donna L. Whitney[2], and Andreas Mulch[1,5]

[1]Senckenberg Biodiversity and Climate Research Centre, Senckenberg, 60325 Frankfurt am Main, Germany
[2]Department of Earth and Environmental Sciences, University of Minnesota, Minneapolis, Minnesota 55455, USA
[3]Institut des Sciences de la Terre (ISTerre), OSUG, Université Grenoble Alpes, CS 40700, 38058 Grenoble, France
[4]Department of Earth and Environmental Sciences, University of Pennsylvania, Philadelphia, Pennsylvania 19104, USA
[5]Institute of Geosciences, Goethe University Frankfurt, 60438 Frankfurt, Germany

ABSTRACT

Continued Africa-Eurasia convergence resulted in post–11 Ma surface uplift of the Central Anatolian Plateau (CAP) and the westward escape of the Anatolian microplate. Contemporaneously, a central Anatolian fluvio-lacustrine system developed that covered extensive parts of the rising CAP. Today, the semi-arid CAP interior—except for the Konya closed catchment—drains toward the Black Sea, the Mediterranean Sea, and the Persian Gulf. Lake connectivity and drainage patterns of the fluvio-lacustrine system in the evolving plateau region are, however, largely unknown.

Here, we present sedimentological and stable isotopic ($\delta^{13}C$ and $\delta^{18}O$) data ($N = 665$) from 13 well-dated lake sections covering the former fluvio-lacustrine depocenters of the southern CAP. Persistently (>1 m.y.) stable paleoenvironmental and hydrological conditions suggest that a low-relief environment characterized the southern CAP during plateau uplift. Throughout the late Miocene, various open and closed lakes of the southern CAP drained into closed, terminal lakes within the plateau interior. Sedimentation east of the Tuz Gölü fault ceased during the early Pliocene (ca. 5.3–3.6 Ma), when the eastern CAP became connected to marine base level as a result of river incision shortly after the switch from regional compression to extension. A final phase of lacustrine carbonate sedimentation characterizes most sampled basins, yet occurred asynchronously over the extent of the CAP. Therefore, the final episode of lacustrine sedimentation is unlikely to have been the result of a climatic event, consistent with the absence of a clear aridification trend in the lacustrine $\delta^{18}O$ data. Rather, capping carbonates reflect the interplay of surface uplift and transition from inward- to outward-drained plateau regions and concomitant lake reorganization during the formation of the CAP and its margins.

INTRODUCTION

The world's largest orogenic plateaus, the Puna-Altiplano and the Tibetan Plateau, are characterized by internally draining basins that persist under arid conditions in the rain shadow of orographic barriers at the plateau margins. Protracted rapid shortening and high surface uplift rates under arid conditions prevent fluvial systems from defeating the internally drained plateau regions, thereby providing a way for internally drained conditions to develop and persist (e.g., Sobel et al., 2003; Strecker et al., 2007).

At a smaller scale, the Pontide and Tauride mountains (Fig. 1A) border the semiarid Central Anatolian Plateau (CAP, Turkey; average elevation ~1 km; Fig. 1A) to its north and south, respectively. Both mountain belts exhibit humid conditions on their windward sides toward the Black Sea and Mediterranean Sea. The onset of the rise of the CAP after ca. 11 Ma (Meijers et al., 2018b) was followed by surface uplift of the Pontide and Tauride Mountains after ca. 8 Ma (Cosentino et al., 2012; Yıldırım et al., 2011; Meijers et al., 2018b). Following a period of compression, central Anatolia has been under an extensional tectonic regime roughly since the Miocene-Pliocene boundary (ca. 5.3 Ma; Jaffey and Robertson, 2005; Rojay and Karaca, 2008; Fernández-Blanco et al., 2013; Özsayin et al., 2013). Today, the CAP is characterized by a bimodal drainage system. The CAP region roughly west of the Tuz Gölü fault (Fig. 1A) is characterized by the internally drained Konya closed catchment (Fig. 1A), which includes the highly evaporative Tuz Gölü (Turkish for "Salt Lake"). The remainder of the CAP is externally drained, by means of rivers flowing into the Black Sea, Mediterranean Sea, and Persian Gulf (Fig. 1A).

Active continental sedimentation has occurred in numerous central Anatolian basins since the late Oligocene (Fig. 1C; e.g., Leng et al., 1999; Ocakoğlu, 2002; Önal et al., 2004; Lüdecke et al., 2013; Mazzini et al., 2013; Meijers et al., 2016, 2018a, 2018b). Paleoenvironmental conditions of fluvio-lacustrine sedimentation and of the development of the central Anatolian lake system can presently be retrieved from the now-incised former depocenters.

Here, we present a comprehensive body of sedimentological data and stable isotope values ($\delta^{18}O$ and $\delta^{13}C$, $N = 665$, including 564 new $\delta^{13}C$ values) from 13 fluvio-lacustrine sections within the southern

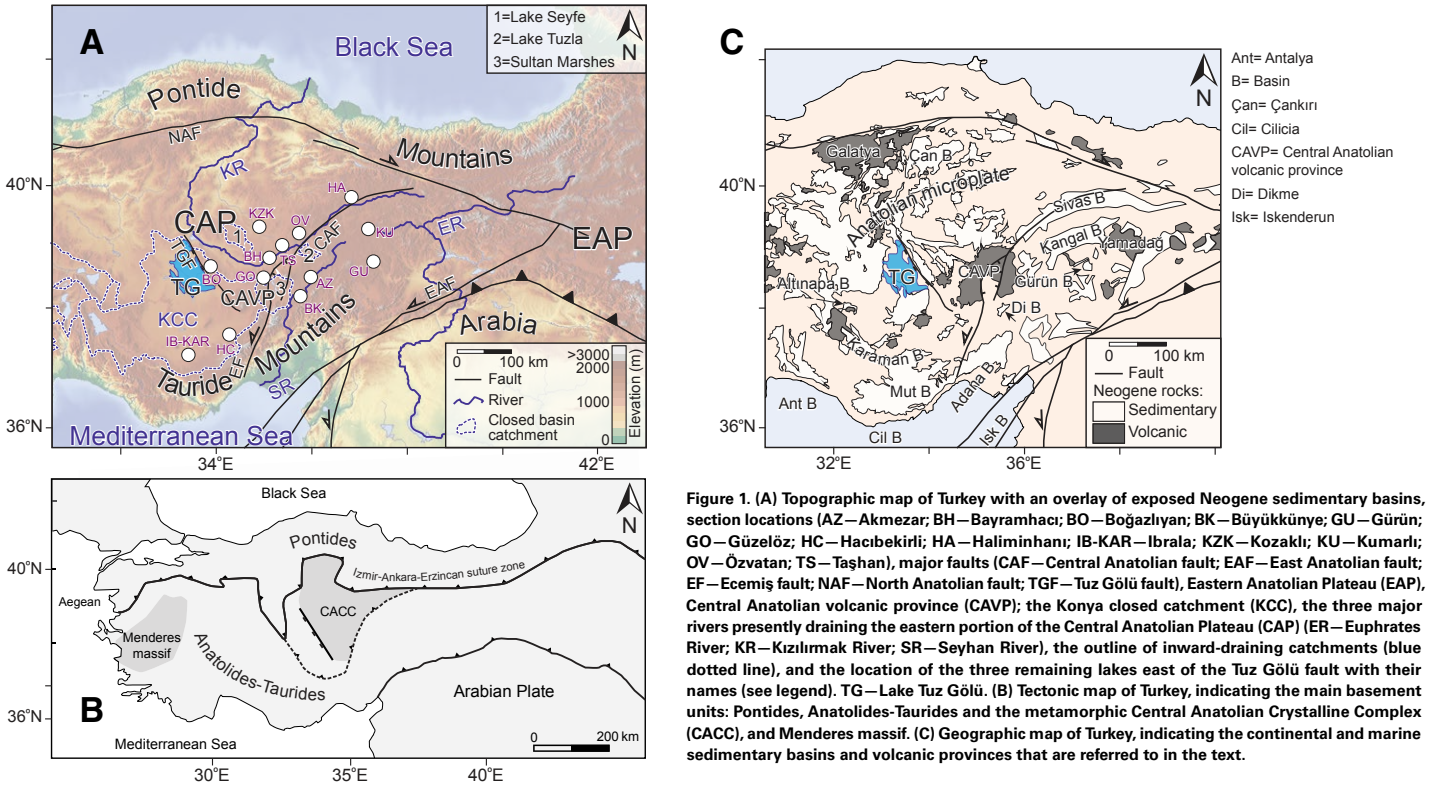

Figure 1. (A) Topographic map of Turkey with an overlay of exposed Neogene sedimentary basins, section locations (AZ—Akmezar; BH—Bayramhacı; BO—Boğazlıyan; BK—Büyükkünye; GU—Gürün; GO—Güzelöz; HC—Hacıbekirli; HA—Haliminhanı; IB-KAR—Ibrala; KZK—Kozaklı; KU—Kumarlı; OV—Özvatan; TS—Taşhan), major faults (CAF—Central Anatolian fault; EAF—East Anatolian fault; EF—Ecemiş fault; NAF—North Anatolian fault; TGF—Tuz Gölü fault), Eastern Anatolian Plateau (EAP), Central Anatolian volcanic province (CAVP); the Konya closed catchment (KCC), the three major rivers presently draining the eastern portion of the Central Anatolian Plateau (CAP) (ER—Euphrates River; KR—Kızılırmak River; SR—Seyhan River), the outline of inward-draining catchments (blue dotted line), and the location of the three remaining lakes east of the Tuz Gölü fault with their names (see legend). TG—Lake Tuz Gölü. (B) Tectonic map of Turkey, indicating the main basement units: Pontides, Anatolides-Taurides and the metamorphic Central Anatolian Crystalline Complex (CACC), and Menderes massif. (C) Geographic map of Turkey, indicating the continental and marine sedimentary basins and volcanic provinces that are referred to in the text.

CAP (Fig. 1A, Table 1) that aims at understanding the hydrology and paleoenvironmental setting of the former depocenters. Ages of deposition are derived from radiometric and magnetostratigraphic ages (e.g., Meijers et al., 2018a, 2018b) and combined with data from (mammal) biostratigraphy (e.g., The NOW Community, 2017). The presented study includes observations and stable isotope data from one section sampled in an early Miocene basin and twelve sections sampled in late Miocene to Pliocene basins of the southeastern CAP. Based on our observations and stable isotope data of the late Neogene depocenters, we discuss lake distribution and connectivity, the paleoenvironmental setting, and the switch from internal to external drainage during times of a changing tectonic regime, surface uplift, and the westward tectonic escape of the Anatolian microplate.

GEOLOGY OF ANATOLIA

The Pontide and Tauride Mountains that border the CAP locally exceed elevations of 3 km, and their steep slopes contrast with the subdued topography of the plateau interior. Owing to its position within the Africa-Eurasia convergence zone, Turkey consists of an amalgamation of geologic terranes. The Pontide Mountains are part of a Late Cretaceous to Paleogene fold-and-thrust belt with a basement of Variscan origin (Okay and Tüysüz, 1999). The Tauride Mountains are underlain by Pan-African basement (Kröner and Şengör, 1990) of the Anatolides-Taurides and are a fold-and-thrust belt of latest Cretaceous to Eocene age (Monod, 1977; Demirtaşlı et al., 1984; Özgül, 1984). The Anatolides-Taurides are separated from the Pontides by the Izmir-Ankara-Erzincan suture zone (Fig. 1B). The basement below most of the CAP consists of the Central Anatolian Crystalline Complex (Fig. 1B), which exposes metamorphic, ophiolitic, and igneous rocks (e.g., Whitney and Hamilton, 2004).

The Neogene sedimentary cover of the CAP includes marine and continental basins. After the deposition of the youngest marine rocks on the plateau interior during the middle Miocene (ca. 12–11 Ma; Poisson et al., 2016; Ćorić et al., 2012; Ocakoğlu et al., 2002), fluvio-lacustrine conditions prevailed. The continental sedimentary rocks are commonly intercalated with volcanic rocks (tuffs, ignimbrites, basalt) that are derived from a number of volcanic provinces. These include the middle Miocene and younger Yamadağ, Galatia, and Central Anatolian volcanic provinces (Fig. 1C; e.g., Wilson et al., 1997,

TABLE 1. SAMPLED AND LOGGED SECTIONS WITH CARBON AND OXYGEN STABLE ISOTOPE RECORDS

Section name (reference code)	Sample code	Number of analyzed samples	Mean age (Ma)	Δ age (m.y.)	Location	
					Latitude (°N)	Longitude (°E)
Bogazliyan (BO)	BO	22	3.9	0.2	38.61101	33.88422
Güzelöz (GO)	GO	21	4.0	0.5	38.39853	34.97129
Özvatan (OV)	OV	72	5.2	0.6	39.14984	35.76082
Büyükkünye (BK)	BK	49	5.4	0.5	38.16070	35.82721
Akmezar (AZ)	AZ	40	5.9	0.6	38.45937	35.99748
Hacibekirli (HC)	10HB	98	6.2	0.8	37.52620	34.35944
Kumarli (KU)	KU	101	6.4	1.1	39.20495	37.19937
Haliminhani (HA)	HA	76	7.9	1.1	39.73006	36.83375
Kozakli (KZK)	KZK	36	7.2	0.4	39.21304	34.87323
Tashan (TS)	TS	35	7.3	0.6	38.93407	35.41439
Bayramhaci (BH)	BH	38	9.5	0.6	38.79650	34.98858
Ibrala (IB-KAR)	IB-KAR	33	11.0	1.0	37.20636	33.38510
Gürün (GU)	GU	44	18.7	1.5	38.72350	37.31461

Notes: We refer to Supplementary Table S1 (see text footnote 1) for all stable isotope results. Sample code refers to the labeling of the samples for each section. Δ age refers to the time intervals below and above the "Mean age" that are (approximately) represented in each section.

Gürsoy et al., 2011, Aydar et al., 2012), which have in part a well-developed volcanic stratigraphy (Central Anatolian volcanic province ignimbrites between ca. 9 and 2.5 Ma; Aydar et al., 2012).

The presence of steep and narrow pre–late Miocene paleorelief in central Anatolia is evidenced by the results of sedimentary provenance studies in the region surrounding the Ecemiş fault segment of the Central Anatolian fault (Fig. 1A; Jaffey and Robertson, 2005). Extremely steep, deeply incised middle Miocene paleovalleys are found buried under continental series many hundreds of meters thick in the Gürün (Fig. 1C; Önal et al., 2004) and Dikme basins (Fig. 1C; Ocakoğlu, 2002), as well as along the Aksu River paleovalley. In the Mut Basin, paleovalleys are concealed by hundreds of meters of estuarine and marine sediments (Bassant et al., 2005; Eriş et al., 2005). Palynological assemblages with mountain-derived flora further suggest that these steep-relief areas locally attained substantial elevations (Akgün et al., 2007). Regional surface uplift of the CAP has occurred since ca. 11 Ma, and the development of orographic barriers along the Pontide and Tauride Mountains after ca. 8 Ma shaped the present-day Anatolian topography and climate (Figs. 2B, 2C; e.g., Yıldırım et al., 2011; Cosentino et al., 2012; Meijers et al., 2018b; Öğretmen et al., 2018).

The modern CAP is cross-cut by a number of transtensional and transpressional faults, most prominently the North Anatolian, East Anatolian, Central Anatolian, and Tuz Gölü faults. The North Anatolian and East Anatolian faults facilitate the present-day westward escape of the Anatolian microplate (Figs. 1A, 1B; McKenzie, 1976). Following distributed shortening during the late Miocene, the sedimentary basins of the CAP have recorded extensional deformation since ca. 5.3 Ma (i.e., the Miocene to Pliocene transition; e.g., Jaffey and Robertson, 2005; Rojay and Karaca, 2008; Fernández-Blanco et al., 2013; Özsayin et al., 2013).

MIOCENE TO PLIOCENE ANATOLIAN PALEOENVIRONMENT AND PALEOCLIMATE

The Pontide Mountains and Tauride Mountains orographic barriers that separate the CAP interior from the Black Sea and Mediterranean Sea, respectively, presently control climatic conditions in Anatolia (Fig. 1A; Schemmel et al., 2013).

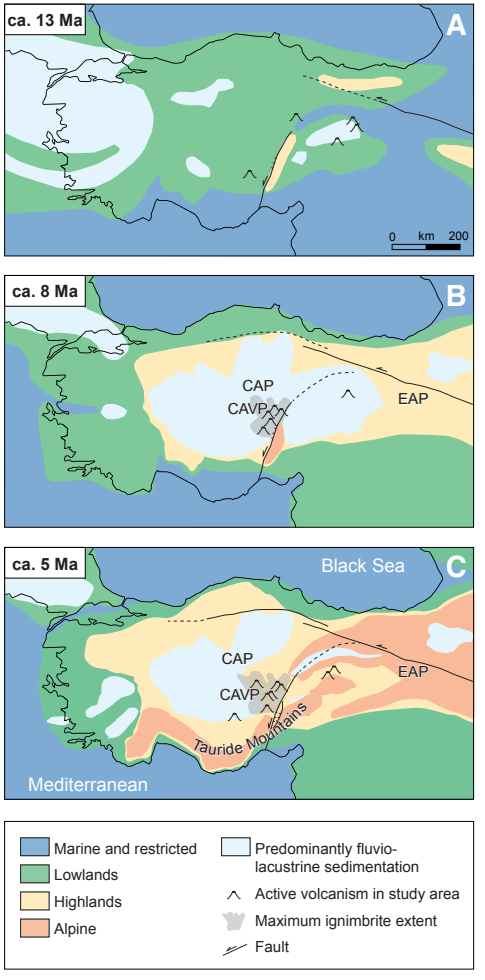

Figure 2. Paleogeographic sketches of Anatolia with present-day coastlines at ca. 13 Ma (A), ca. 8 Ma (B), and ca. 5 Ma (C). Volcanic activity in the area that is the subject of this study is based on the compilation by Schleiffarth et al. (2018); volcanics with ages within ±1 m.y. of the age of the paleogeographic sketches were included. Areas with predominantly fluvio-lacustrine sedimentation do not necessarily represent connected basins. The maximum extent of ignimbrites that were emplaced at ca. 8 Ma and ca. 5 Ma was derived from Le Pennec et al. (1994). Paleogeographic sketches are after Huang et al. (2019). Main faults affecting the study area were added following Jaffey and Robertson (2001), Ocakoğlu (2004), Şengör et al. (2005), and Yıldırım et al. (2011). CAP—Central Anatolian Plateau; EAP—Eastern Anatolian Plateau; CAVP—Central Anatolian volcanic province.

Mean annual precipitation (MAP) decreases from ~1000–1500 mm on the windward sides of both ranges to 300–500 mm within the plateau interior. Mean annual temperatures (MATs) along the Black Sea coast of 13 °C are lower than MAT of 20 °C along the Mediterranean coast, while MAT averages 4–10 °C within the plateau interior.

During the early to middle Miocene, central Anatolia was characterized by a humid, subtropical climate (Akgün et al., 2007). A review of floral data sets indicates MATs of 17–21 °C from the late early Miocene to the late middle Miocene, after which MATs dropped through the late Miocene to 13–17 °C during the early Pliocene (Kayseri-Özer, 2017). Meanwhile, MAPs ranged between 1000 mm to 1400 mm from the late early Miocene to the Pliocene, with an intermittent period of lower values of ~900 mm during the late to latest Miocene (Kayseri-Özer, 2017).

Vegetation reconstructions based on phytolith data indicate a mosaic of open-habitat grassland, woodland, and forest vegetation in central Anatolia during the Miocene (Strömberg et al., 2007). Phytolith and palynofloral records further indicate that open-habitat grasslands became increasingly dominant during the late Miocene (Akgün et al., 2007; Strömberg et al., 2007), consistent with mammal dental ecometrics and faunal similarity pattern data (Kaya et al., 2018). Along with the dominantly open-habitat grasslands, paleovegetation reconstructions indicate the presence of a large variety of other vegetation types covering central Anatolia during the Messinian (ca. 7.2–5.3 Ma), such as mixed mesophytic forests, broad-leaved evergreen forests, evergreen needleleaf forests, and xeric open woodlands or steppes, as well as areas with high percentages of zonal herb components (Kayseri-Özer, 2017; Denk et al., 2018). The abundance of mid-elevation conifers in the late Miocene (post–9 Ma) to Pliocene pollen record of the Çankırı Basin is consistent with elevations of ~940–2000 m (Fig. 1C; Yavuz et al., 2017). During the Pliocene, the relative abundance of the sclerophyllous, legume-like and zonal herb components increased over Anatolia; a relative increase of broad-leaved components in central Anatolia with respect to western Anatolia has been interpreted to result from higher central Anatolian topography (Kayseri-Özer, 2017).

During the late Miocene, central Anatolia formed part of the Old World savannah paleobiome, which harbored the Pikermian chronofauna (Kaya et al., 2018). The post-Miocene demise of the Old World savannah paleobiome in the Anatolian region was possibly caused by an increase in humidity (Kaya et al., 2018), which may be reflected in the increase of MAP across the Miocene-Pliocene boundary (Kayseri-Özer, 2017).

Presently, the highly evaporative Tuz Gölü is one of the few remaining lakes in central Anatolia. Continental sedimentation within the Tuz Gölü Basin has been ongoing since the Tortonian (Fernandez-Blanco et al., 2013). The Tuz Gölü Basin is presently the terminal lake of the Konya closed catchment (Fig. 1A), with its subdued topography and elevations of ~850–1100 m. The Konya closed catchment is fed by surface and ground water from the Tauride Mountains (Üstün et al., 2015). During wetter periods, in particular during interglacials, it hosted extensive "pluvial lakes", the last of which remained in existence well into the Holocene; (e.g., Leng et al., 1999; Jones et al., 2007; Dean et al., 2013). The Konya closed catchment is separated from the eastern CAP by the Tuz Gölü fault (Fig. 1A). The eastern CAP (i.e., the portion east of the Tuz Gölü fault) attains overall higher elevations and hosts only a handful of small, closed and commonly fault-bounded evaporative basins in which lacustrine deposition continues (Lake Seyfe, Lake Tuzla, and the Sultan Marshes; Figs. 1A, 1C). The last episode of widespread lacustrine deposition occurred during the early Pliocene (Fig. 2C; Meijers et al., 2018b). River incision subsequently led to drainage of these former lacustrine areas toward all surrounding terminal sediment sinks, namely the Mediterranean Sea (via the Seyhan River), the Persian Gulf (via the Euphrates River), and the Black Sea (via the Kızılırmak River; Fig. 1A).

APPROACH AND METHODS

Twelve (12) middle Miocene to Pliocene continental sedimentary sections (Fig. 3) within the southern CAP were sampled for carbon ($\delta^{13}C$) and oxygen ($\delta^{18}O$) stable isotopes. Levels sampled for stable isotopes include lacustrine carbonates as well as marls, and calcareous claystones and siltstones. We evaluate the distribution and age range of the sampled basins as well as their $\delta^{13}C$ and $\delta^{18}O$ data alongside the stable isotope results obtained from the Kangal Basin (Kumarlı section; Meijers et al., 2018a). The age interval covered by each section is presented in Figure 4. For the chronologies of the sampled Miocene to Pliocene fluvio-lacustrine sedimentary rocks, we refer to Meijers et al. (2018a, 2018b). In summary, the chronologies are based on radiometric ages, magnetostratigraphy, and (mammal) biostratigraphy. The indispensable chronologies allow us to interpret the sedimentological observations and stable isotope results within a reliable temporal framework.

Sedimentary Characterization of the Miocene to Pliocene Central Anatolian Lake System

Twelve (12) sections (Fig. 3) were logged in the field by determining the rock type of each bed or sequence of beds (including clast type for coarse-grained sedimentary rocks as well as for ignimbrites). Stratigraphic thicknesses were measured using a TruPulse laser range finder (except for the Gürün and Hacıbekirli sections, for which a measuring stick was used) and dip corrected to obtain true stratigraphic thicknesses. Periodic recalibration to a reference base point indicates a cumulative thickness error of <1 m over the entire thickness of each section. The stratigraphic nomenclature (i.e., the named geologic formations and members used in the Results section) is based on the 1:100,000-scale geological maps of the General Directorate of Mineral Research and Exploration of Turkey (MTA, 2019).

Carbon and Oxygen Stable Isotope Geochemistry

A total of 564 samples were taken from carbonate-bearing levels of 12 measured sections. All $\delta^{18}O$ results were reported in summary fashion in Meijers et al. (2018b). $\delta^{13}C$ and $\delta^{18}O$ results for the Kumarlı section (N = 101) were reported in

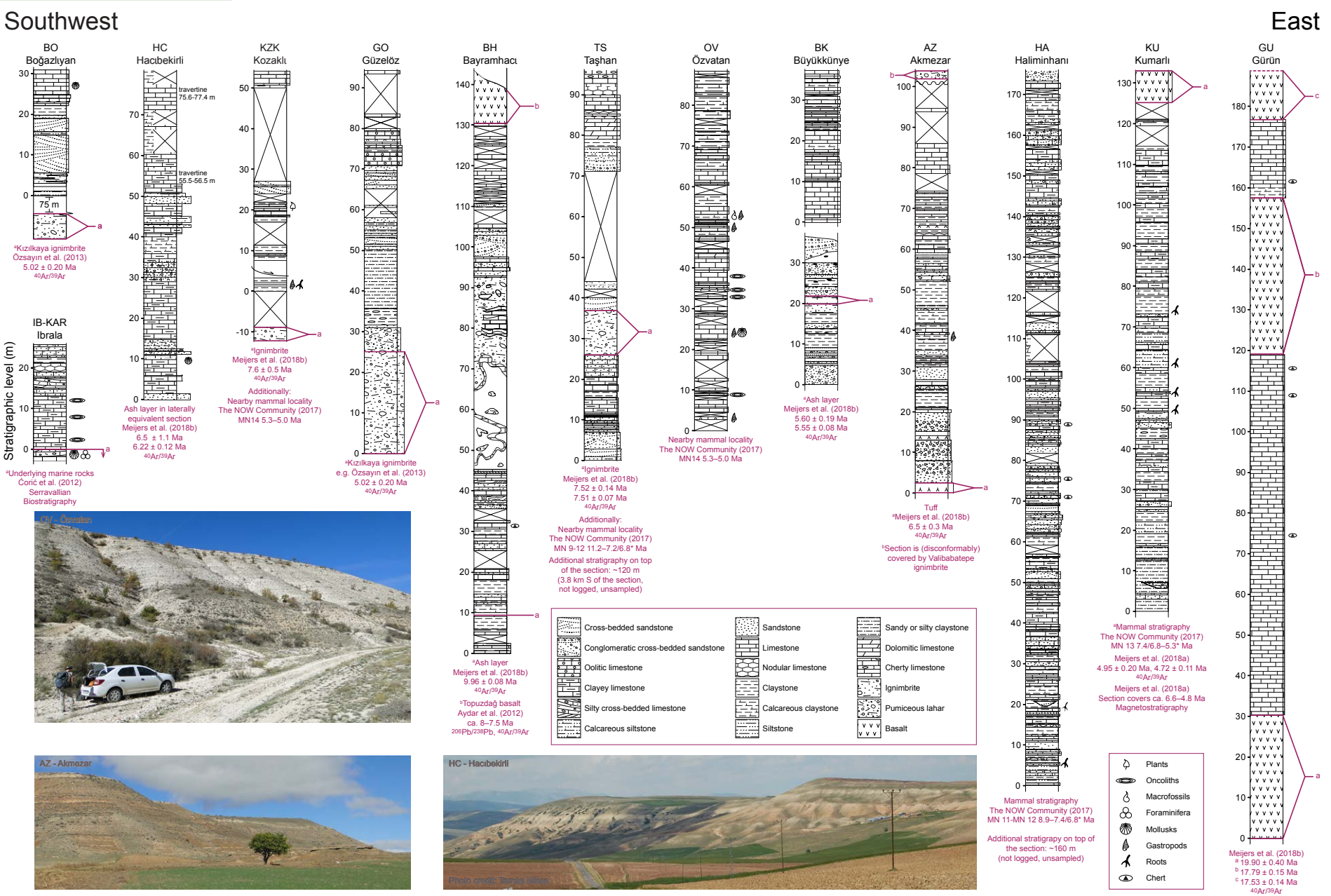

Figure 3. Stratigraphic logs of the 12 sampled sedimentary sequences and the Kumarlı section, Central Anatolian Plateau, Turkey, as well as their age constraints and photos of the Özvatan, Akmezar, and Hacıbekirli sections. Photo credit (section HC): Tamás Mikes. Asterisk (*): The dash between 7.4 and 6.8 Ma (7.4/6.8 Ma) indicates the uncertainty in the age of the MN12-MN13 boundary.

Meijers et al. (2018a). Here we plot all $\delta^{13}C$ and $\delta^{18}O$ data alongside their corresponding stratigraphic logs (Fig. 5) with the ultimate aim of establishing common patterns of lake development across the evolving CAP. After drilling the finest component of the whole-rock samples in the laboratory, sample powders were digested in orthophosphoric acid and analyzed as CO_2 in continuous-flow mode using a Thermo MAT 253 mass spectrometer interfaced with a Thermo GasBench II at the Joint Goethe University– Senckenberg BiK-F Stable Isotope Facility, Institute of Geosciences, Goethe University Frankfurt, Germany. The analytical procedures follow Spötl and Vennemann (2003). Raw isotopic ratios were calibrated against NBS 18 and NBS 19 carbonate reference materials and against a Carrara marble in-house standard. Final $\delta^{18}O$ and $\delta^{13}C$ values are reported against Vienna standard mean ocean water (V-SMOW) and Vienna Peedee belemnite (V-PDB), respectively, with analytical uncertainties that are typically <0.10‰ ($\delta^{18}O$) and <0.07‰ ($\delta^{13}C$). The uncertainties are based on the standard deviations of the reference materials over the course of the measurements. Carbonate contents were derived from standard to sample total peak area comparison and uncertainties are <10% absolute (see Supplemental Table S1[1]). Covariance between $\delta^{13}C$ and $\delta^{18}O$ was determined using the Pearson correlation coefficient (Table S1). The significance of the calculated covariance is determined by the (*N*-dependent) critical value. The critical value decreases asymptotically with *N*, for which we set the significance level to 95% (see the "Critical values" sheet in Table S1). Only intervals that display a significant covariance at the 95% level are listed in the Results section. Standard deviations of all obtained $\delta^{13}C$ and $\delta^{18}O$ values for each section refer to 1σ uncertainties.

Fig. S1. Pictures of the Büyükkünye section (BK), which indicates the location of the two subsections. The lower subsection consists of clastic sedimentary rocks and paleosols. The upper subsection consists of lacustrine carbonates and was mined for its carbonates.

[1]Supplemental Material. File S1: Extent and connectivity of the lakes based on the stable isotopic record; Figure S1: Pictures of the two subsections of the Büyükkünye section; Figure S2: Satellite imagery of the Zamantı River valley showing the Valibabatepe ignimbrite draping preexisting topography; Figure S3: Picture and satellite imagery of the Özvatan section showing the clastic alluvial fan deposits toward its top; Table S1: All individual $\delta^{18}O$ and $\delta^{13}C$ results and covariance analysis; and Supplemental KML: KML file with GPS points. Please visit https://doi.org/10.1130/GES02135.S1 or access the full-text article on www.gsapubs.org to view the Supplemental Material.

RESULTS

Sedimentary Facies and Environmental Depositional Setting of the Miocene to Pliocene Central Anatolian Lake System

All sections are characterized by shallowly dipping to horizontal bedding planes. For the locations of the sections, stratigraphic logs, age constraints, and $\delta^{13}C$ and $\delta^{18}O$ values, we refer to Figures 1 and 3–6, Table S1 (footnote 1), and the Supplemental KML file (footnote 1). For detailed information about the sampled age intervals of each section, we refer to Meijers et al. (2018a; 2018b). To ease the retrieval of information for each section, we describe the sedimentology and the stable isotope results of the sections below in alphabetical order.

Akmezar (AZ)

Ürgüp Formation
Logged interval: 104 m; sampled interval: 20.0–93.5 m, *N* = 40

The lowest part of the Akmezar section (0–20 m) consists of mafic volcanoclastic tuffs (Göbü tuff; 6.5 ± 0.3 Ma, $^{40}Ar/^{39}Ar$ on plagioclase; Meijers et al., 2018b) and detrital volcanic tuff that contains olivine and feldspar phenocrysts as well as serpentinite clasts. The 20–93.5 m interval consists of an alternation of sandstones, claystones, marls, (argillaceous) carbonates, and soils with a prismatic structure. Following an unexposed interval between 93.5 and 102 m, the top of the section is capped by the ca. 2.6 Ma Valibabatepe ignimbrite (2.52 ± 0.49 Ma and 2.73 ± 0.08 Ma, $^{40}Ar/^{39}Ar$ on plagioclase; Aydar et al. [2012] and Higgins et al. [2015], respectively). The normal magnetic polarity of the ignimbrite elsewhere in the Central Anatolian volcanic province (Piper et al., 2013) very likely constrains its emplacement to within chron C2An.1n (3.032–2.581 Ma; Hilgen et al., 2012).

The mean $\delta^{13}C$ value is –7.1‰ ± 1.8‰ and the mean $\delta^{18}O$ value is 21.9‰ ± 0.7‰ for the sampled interval (73.5 m, *N* = 40). The interval from 58 to 93 m displays a significant negative covariance between $\delta^{13}C$ and $\delta^{18}O$.

Bayramhacı (BH)

Tuzköy Formation and Ürgüp Formation (Kışladağ Limestone Member)
Logged and sampled interval: 130 m, *N* = 38

The Bayramhacı section is an alternation of sandstones, lacustrine limestones, argillaceous

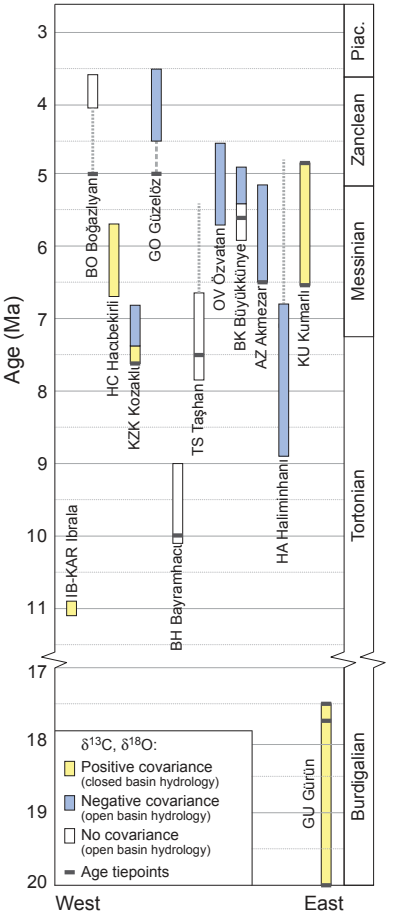

Figure 4. Schematic overview of the age interval covered by each section. Dark gray horizontal dashes indicate age constraints obtained within each section, either through magnetostratigraphy (section KU; Meijers et al., 2018a), $^{40}Ar/^{39}Ar$ dating (sections BO, KZK, GO, BH, TS, BK, AZ, and GU; Meijers et al., 2018b), or mammal stratigraphy (section HA; e.g., The NOW Community, 2017; Kaya and Kaymakçı, 2013). Dashed line indicates the logged but unsampled interval between the dated ignimbrite and the isotopic section (section GO); dotted gray lines indicate the interval that is likely covered by the unsampled interval above a measured section (sections TS and HA; assumed sedimentation rate: 7.5 cm/k.y.) or below a measured section (section BO; assumed sedimentation rate: 8.0 cm/k.y.). Colors indicate whether $\delta^{18}O$ and $\delta^{13}C$ show a positive, negative, or no covariance (see figure for legend). Piac.—Piacenzian.

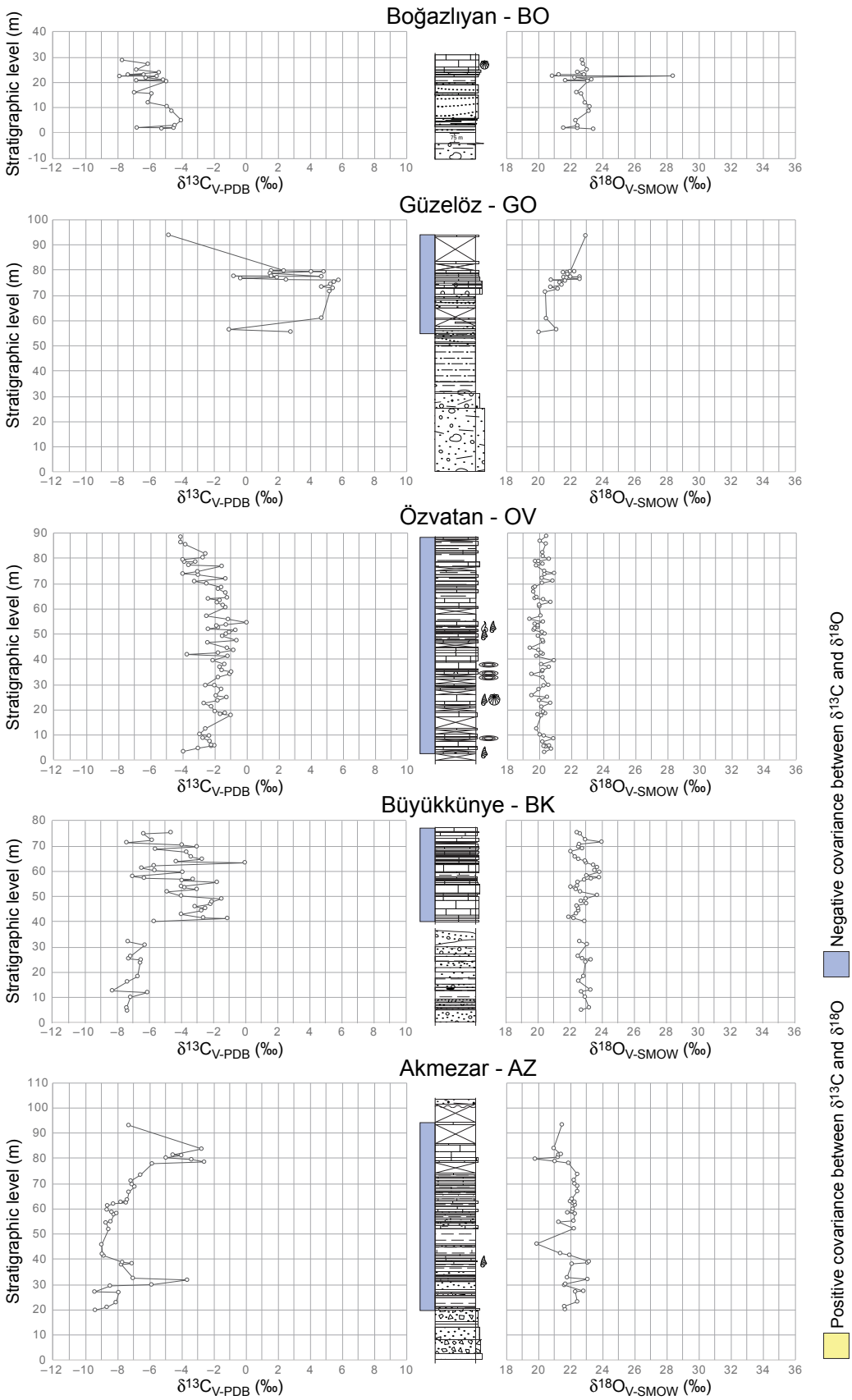

Figure 5. Stratigraphic logs and $\delta^{18}O$ and $\delta^{13}C$ values for all sampled sections, ordered from old (bottom) to young (top). Sections may overlap in age. Legend for the stratigraphic logs is as in Figure 3. V-PDB—Vienna Peedee belemnite; V-SMOW—Vienna standard mean ocean water. (*Continued on following two pages.*)

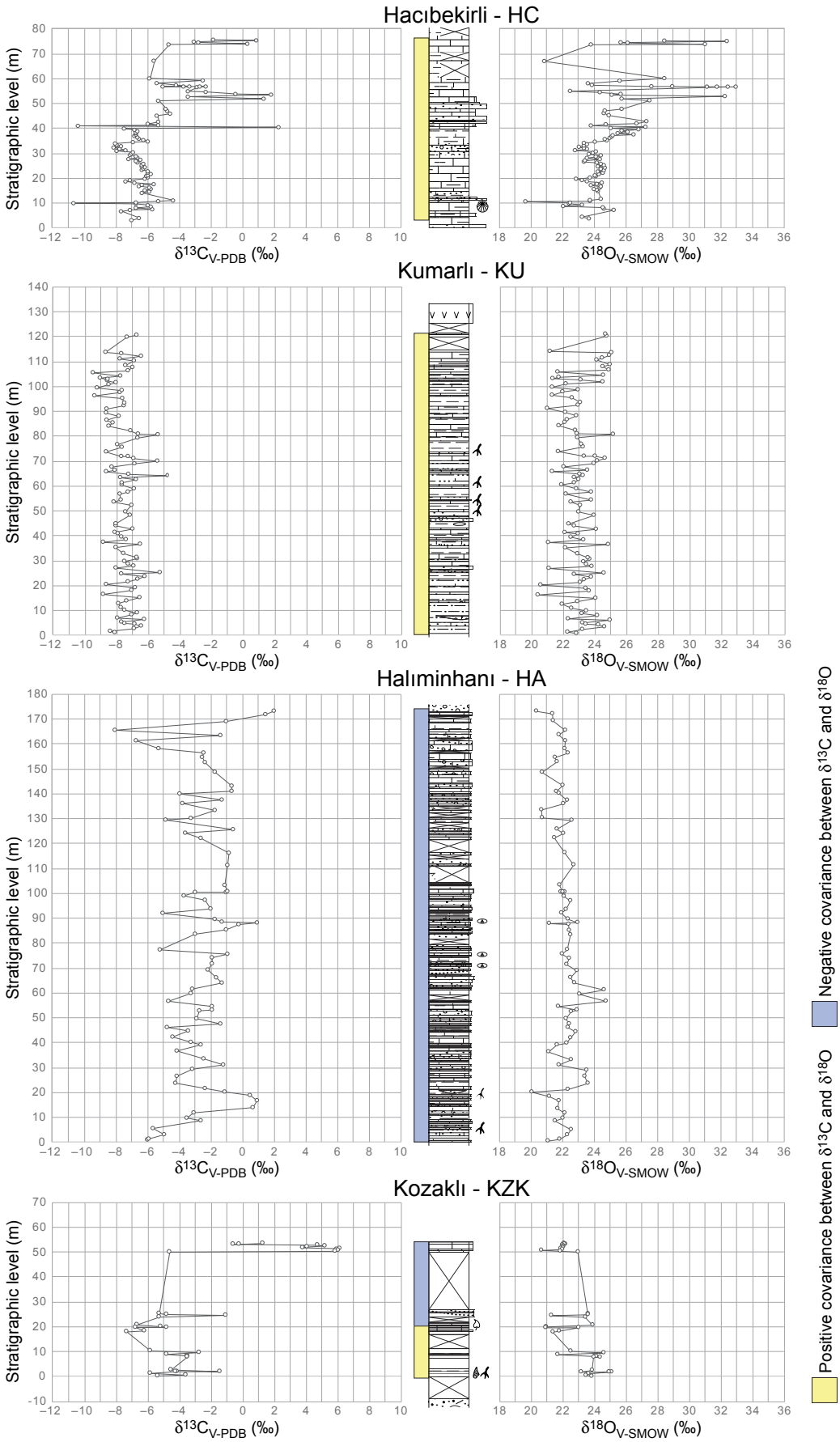

Figure 5 (*continued*).

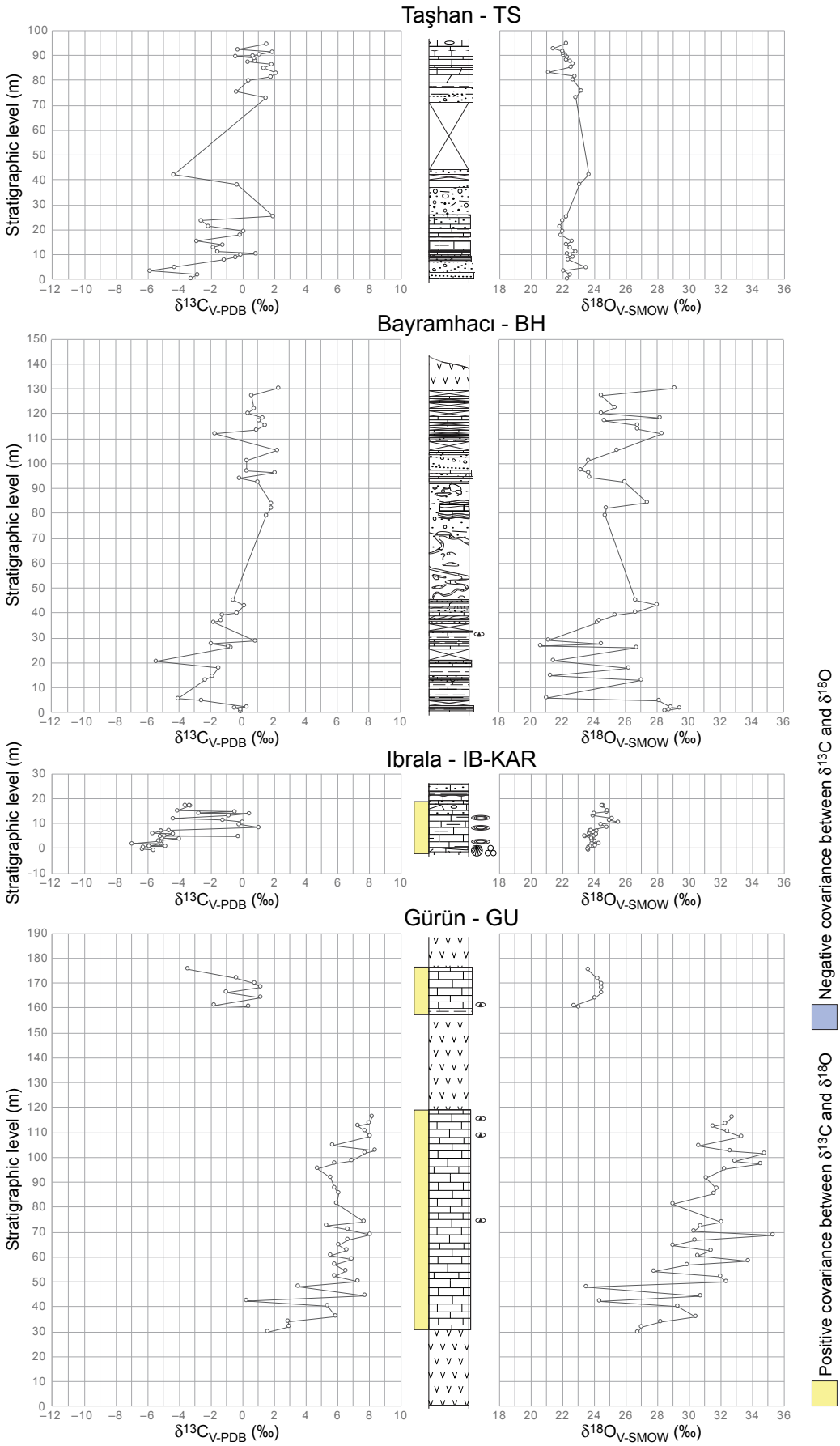

Figure 5 (*continued*).

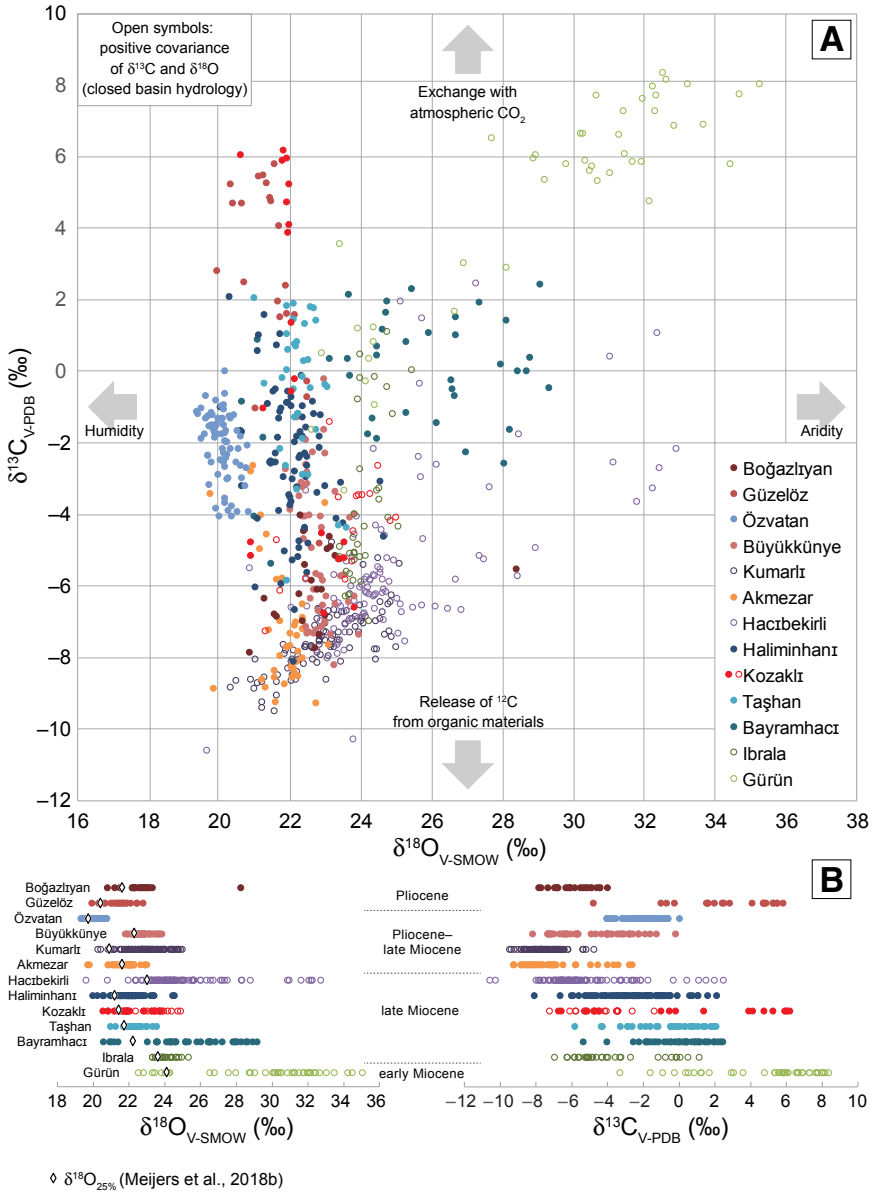

Figure 6. Results of the stable oxygen and carbon isotope analysis. (A) $\delta^{18}O$ versus $\delta^{13}C$ values; a positive covariance between $\delta^{18}O$ and $\delta^{13}C$ indicates hydrologically closed lakes (Leng and Marshall, 2004). Closed symbols are used for sections with a positive covariance between $\delta^{18}O$ and $\delta^{13}C$. (B) Chart displaying all $\delta^{18}O$ and $\delta^{13}C$ values. The $\delta^{18}O_{25\%}$ value for each section (Meijers et al., 2018b) equals the average of the 25% lowest $\delta^{18}O$ values. $\delta^{18}O_{25\%}$ is used as a proxy for pre-evaporative $\delta^{18}O$ values. V-PDB—Vienna Peedee belemnite; V-SMOW—Vienna standard mean ocean water.

limestones, sandy limestones, claystones, and cross-bedded pumice gravel. Minor soft-sediment deformation structures with convolute bedding occur at ~13 m (Fig. 7B) and between 30 and 42 m (10–30 cm thick; Fig. 7C). At ~32 m, the section contains a cherty level. Between 46 m and 92 m, large convolute structures tens of meters across (Figs. 3, 7A) consist of deformed lake sediments and parts of the overlying pumiceous, nonwelded ignimbrite sheet. The deformed lake sediments consist of ripoff masses of up to 5 m thick that are embedded into the main ignimbrite sheet. Samples BH29 to BH31 were retrieved from such embedded lake sediments. An ash layer in the lower part of the section yielded an age of 9.96 ± 0.08 Ma ($^{40}Ar/^{39}Ar$ on biotite; Meijers et al., 2018b).

The 130-m-thick sampled interval ($N = 38$) has a mean $\delta^{13}C$ value of –0.2‰ ± 1.7‰ and a mean $\delta^{18}O$ value of 25.5‰ ± 2.4‰. $\delta^{18}O$ and $\delta^{13}C$ variability below the slumped and disturbed interval (~9‰ and ~6‰, respectively) is higher than above the slumped interval (~6‰ and ~4‰, respectively).

Boğazlıyan (BO)

Peçenek Formation and Kışladağ Limestone Member
Logged and sampled interval: 30.2 m, $N = 22$

The Boğazlıyan section consists primarily of (cross-bedded) sandstones, claystones, and silty claystones. The upper 9 m of the section are formed by limestones, which are in places nodular. 75 m below the base of the section, the Kızılkaya ignimbrite is exposed. The Kızılkaya ignimbrite was dated near the section at 5.02 ± 0.20 Ma ($^{40}Ar/^{39}Ar$ on sanidine; Özsayin et al., 2013).

The mean $\delta^{13}C$ value is –5.9‰ ± 1.1‰ and the mean $\delta^{18}O$ value is 22.8‰ ± 1.4‰ for the 30.2 m sampled interval ($N = 22$). $\delta^{13}C$ values show an overall decreasing trend from the base of the section to the top, from approximately –5 ‰ to –7 ‰, whereas $\delta^{18}O$ values remain relatively constant. The relatively large 1.4‰ standard deviation for $\delta^{18}O$ stems from one sample with $\delta^{18}O = 28.4‰$ (at 22.4 m); omitting this sample reduces the average $\delta^{18}O$ value and uncertainty to 22.5‰ ± 0.7‰.

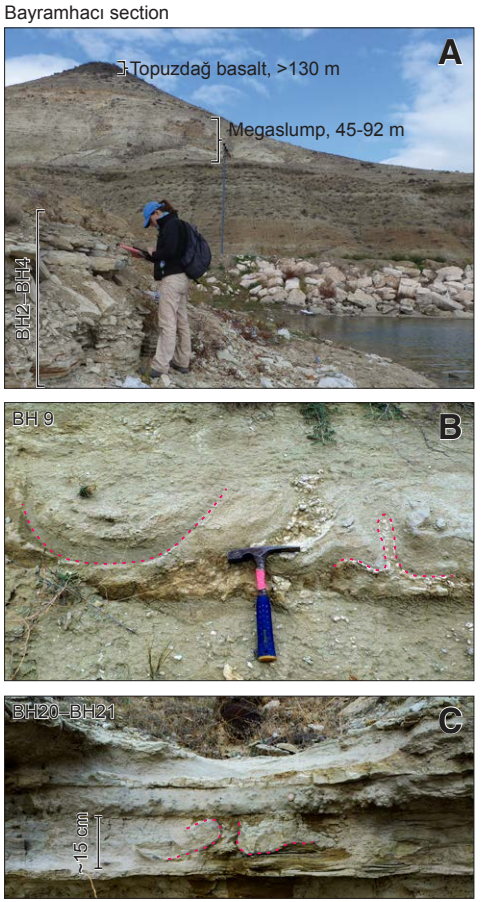

Figure 7. Field photographs of the Bayramhacı section. (A) Section overview, indicating the interval with samples BH2–BH4 at the bottom of the section, the approximate interval of the megaslump, and the Topuzdağ basalt at the top of the section. (B) Convolute bedding at section height ~13 m (sample BH9). (C) Convolute bedding at ~32 m (samples BH20–BH21).

Büyükkünye (BK)

Ürgüp Formation
Logged and sampled interval: 76 m, $N = 49$

The Büyükkünye section comprises two subsections (each 38 m thick; Fig. S1 [footnote 1]) that are separated by an oblique unconformity of uncertain origin (tectonic or erosional). The lower subsection consists of unconsolidated conglomerates with well-rounded limestone cobbles and boulders, as well as claystones, calcareous sandstones, and paleosols. A pumiceous felsic ash layer within the first subsection was dated at 5.55 ± 0.08 Ma and 5.60 ± 0.19 Ma ($^{40}Ar/^{39}Ar$ on amphibole and plagioclase, respectively; Meijers et al., 2018b). The upper subsection consists of travertine and dolomitic, clayey, oncolitic and chalky limestones, as well as a limited number of marl and claystone layers.

Nearby outcrops show that both sections were previously overlain by the now-eroded ca. 2.6 Ma Valibabatepe ignimbrite (Aydar et al., 2012; Higgins et al., 2015).

The lower subsection ($N = 13$) has a mean $\delta^{13}C$ value of –7.0‰ ± 0.6‰ and a mean $\delta^{18}O$ value of 22.9‰ ± 0.3‰. The upper subsection ($N = 36$) has a mean $\delta^{13}C$ value of –4.1‰ ± 1.7‰ and a mean $\delta^{18}O$ value of 22.8‰ ± 0.6‰. The higher standard deviations indicate higher variability within the upper, carbonate-rich units. The upper subsection displays a significant negative covariance between $\delta^{18}O$ and $\delta^{13}C$.

Gürün (GU)

Gürün Formation (Terzioğlu Member)
Logged interval: 175.2 m; sampled interval: 30.0–116.2 m and 160.4–175.2 m, $N = 44$

The Gürün section is located within the Gürün Basin and consists of two white and beige lacustrine carbonate successions between three basalt flows (Karadağ Volcanics; Önal et al., 2004). From the bottom to the top, these basalts were dated at 19.90 ± 0.40 Ma, 17.79 ± 0.15 Ma, and 17.53 ± 0.14 Ma ($^{40}Ar/^{39}Ar$ on whole rock; Meijers et al., 2018b). The lacustrine succession locally consists of marls and dolomite, and in some places contains cherts.

The lowest sampled interval (30.0–116.2 m) yields a mean $\delta^{13}C$ value of 6.0‰ ± 1.8‰ and a mean $\delta^{18}O$ value of 30.8‰ ± 2.6‰. The upper sampled interval (160.4–175.2 m) yields a mean $\delta^{13}C$ value of –0.3‰ ± 1.6‰ and the mean $\delta^{18}O$ value of 23.8‰ ± 0.7‰. Overall, the section displays a significant positive covariance between $\delta^{13}C$ and $\delta^{18}O$.

Güzelöz (GO)

Ürgüp Formation (Kışladağ Limestone Member)
Logged interval: 94 m; sampled interval: 55.5–93.8 m, $N = 21$

The sampled Güzelöz section starts just above the ca. 5 Ma Kızılkaya ignimbrite (e.g., Özsayin et al., 2013; Aydar et al., 2012) with a 6-m-thick pumiceous lahar (25–31 m) that reworks the underlying ignimbrite. It is overlain by an ~40-m-thick interval of (cross-bedded) sandstones, silty mudflows, reworked ignimbrite, and conglomerate. Within this interval, paleosols alternate with mudflows and calcarenites. Toward the top of the section (71–94 m), the presence of chalky, oolitic and massive limestones alternating with unexposed intervals suggests a lower-energy lacustrine depositional environment.

The mean $\delta^{13}C$ value is –2.7‰ ± 2.8‰ and the mean $\delta^{18}O$ value is 21.5‰ ± 0.7‰ for the 38-m-thick sampled interval ($N = 21$). $\delta^{13}C$ and $\delta^{18}O$ display significant negative covariance.

Hacıbekirli (HC)

İnsuyu Formation (Kızılbayır Member and Katrandedetepe Member)
Logged and sampled interval: 77.4 m, $N = 98$

The Hacıbekirli section is an alternation of limestones, sandy, silty, or clayey limestones, rare (cross-bedded) sandy limestones, and (uncemented) conglomerates, as well as marls, claystones, clayey sandstones, and calcareous sandstones. Travertine occurs toward the top of the section, from which no stable isotope data are presented here. A tuffite in a laterally equivalent section (37.742806°N, 34.740091°E) yielded $^{40}Ar/^{39}Ar$ ages of 6.5 ± 1.1 Ma (total fusion, plagioclase) and 6.22 ± 0.12 Ma (plateau age, amphibole; Meijers et al., 2018b). We rely on the latter for stratigraphic correlation of the Hacıbekirli section. The beds of the Hacıbekirli section are gently tilted to the WNW (302°/12°, dip direction and dip angle).

The $\delta^{13}C$ and $\delta^{18}O$ values ($N = 98$) average –5.4‰ ± 2.3‰ and 25.1‰ ± 2.4‰ and show a significant positive covariance throughout the section.

Haliminhanı (HA)

Incesu Formation
Logged and sampled interval: 176 m, *N* = 76

Located within the Sivas Basin, the stratigraphy of the Haliminhanı section consists of conglomerates, (cross-bedded) sandstones, siltstones, marls, claystones, and limestones. Some levels contain rootlets and cherts. The Haliminhanı section has been extensively studied for mammal stratigraphy, which indicates a MN11–MN12 age (e.g., The NOW Community, 2017; Kaya and Kaymakçı, 2013), i.e., 8.9–7.4/6.8 Ma (Hilgen et al., 2012).

The 76 $\delta^{13}C$ and $\delta^{18}O$ values from the Haliminhanı section do not systematically change from the base to the top of the section, and neither does the internal variability of the $\delta^{13}C$ and $\delta^{18}O$ data. The mean $\delta^{13}C$ value is –2.5‰ ± 1.9‰ and the mean $\delta^{18}O$ value is 22.1‰ ± 0.8‰.

Ibrala (IB-KAR)

İnsuyu Formation
Logged interval: –0.6 to 25.6 m; sampled interval: –0.6 to 17.1 m, *N* = 33

The Ibrala section was sampled in a quarry in the Karaman Basin. It consists almost entirely of lacustrine limestones, in particular chalky, massive, oncolitic and nodular limestones interbedded with thin marly layers. Some layers contain stromatolites. Higher-energy channels scouring the succession are filled with marls and oncolites. The section overlies a sequence of marine, oyster-bearing, nearshore and estuarine deposits of Serravallian age (13.82–11.62 Ma; Ćorić et al., 2012). The gradual, conformable transition from the marine to the continental environment therefore provides a maximum age of ca. 11 Ma (Tortonian) for the sampled continental rocks.

The 33 $\delta^{13}C$ and $\delta^{18}O$ values average –3.8‰ ± 2.3‰ and 24.1‰ ± 0.5‰, respectively; which indicates the rather high variability in the range of $\delta^{13}C$ values (ca. –7‰ to –1‰) in comparison to the $\delta^{18}O$ values. Overall, $\delta^{13}C$ and $\delta^{18}O$ tend to increase toward the top of the section. $\delta^{13}C$ and $\delta^{18}O$ show significant positive covariance.

Kozaklı (KZK)

Kızılırmak Formation and Kozaklı Limestone Member
Logged interval: –12 to 53.6 m; sampled interval: 0–53.6 m, *N* = 36

The Kozaklı section was sampled along a road cut near the town of Kozaklı. Large intervals of the section are unexposed. Its base is defined by the top of a 7.6 ± 0.5 Ma ignimbrite ($^{40}Ar/^{39}Ar$ on plagioclase; Meijers et al., 2018b). The lowest exposed interval (0–10.5 m) consists of claystones that include rootlets, fossils, and gypsum rosettes as well as rare sandstone and limestone layers. The central exposed part of the section (18–26.6 m) includes (calcareous) claystones, (clayey) limestones, and layers rich in organic matter. The upper part of the central part of the section consists of an alternation of (silty) claystones and (cross-bedded) sandstones, including a layer that contains (unsampled) pedogenic carbonate. The top of the section (49.8–53.6 m) consists of clayey limestones that turn into (micritic, oncolitic) limestone beds (beds <10 cm thick) and massive limestones toward the very top. An additional age for the deposits in the sampled basin comes from a nearby mammal locality (MN14, 5.3–5.0 Ma, locality Kozaklı; The NOW Community, 2017).

Carbonate $\delta^{13}C$ values (*N* = 36) vary widely (between –7‰ and +6‰), which is expressed in the high 1σ standard deviation of the average, –2.0‰ ± 4.3‰. The top of the section that consists dominantly of limestone yields significantly higher $\delta^{13}C$ values compared to the rest of the section. The average $\delta^{18}O$ value is 22.8‰ ± 1.2‰, and $\delta^{18}O$ does not change significantly throughout the section. The lower part of the section (0–18.3 m) displays a significant positive covariance between $\delta^{13}C$ and $\delta^{18}O$. The upper part of the section (18.3–53.6 m) displays a significant negative covariance.

Kumarlı (KU)

Kangal Formation and Etyemez Member (member of Kangal Formation), overlain by the Göbekören Basalt
Logged and sampled interval: 0–135 m, *N* = 101

The Kumarlı section is located within the Kangal Basin. A detailed description of the Kumarlı section and the isotopic results are provided in Meijers et al. (2018a). The Kumarlı section consists of an alternation of (carbonaceous) claystones, (clayey) limestones, chalk, and marls, as well as rare conglomerate. Magnetostratigraphy, whole-rock basalt $^{40}Ar/^{39}Ar$ dating, and mammal stratigraphy constrain sediment deposition to between ca. 6.6 and 4.8 Ma (Meijers et al., 2018a).

The average $\delta^{18}O$ value is 23.0‰ ± 1.1‰, and the average $\delta^{13}C$ value is –7.6‰ ± 0.9‰ (*N* = 101). $\delta^{13}C$ and $\delta^{18}O$ display a significant positive covariance.

Özvatan (OV)

İç Anadolu group, Kozaklı Limestone Member
Logged and sampled interval: 89 m, *N* = 72

The Özvatan section consists entirely of chalky, micritic, and rarely dolomitic or oncolitic limestones, in places intercalated with marls. Parts of the section are covered in scree, which likely conceals marly intervals. The age of the section is based on a mammal assemblage dated as MN14 (5.3–5.0 Ma, locality Iğdeli; The NOW Community, 2017) in a time-equivalent section.

The 72 $\delta^{13}C$ and $\delta^{18}O$ values average –2.1‰ ± 0.9‰ and 20.1‰ ± 0.3‰, respectively. $\delta^{13}C$ values roughly increase toward the middle part of the section, followed by a rough decrease toward initial values. $\delta^{13}C$ and $\delta^{18}O$ display a significant negative covariance throughout the section.

Taşhan (TS)

Ürgüp Formation
Logged and sampled interval: 96 m, *N* = 35

The Taşhan section was sampled starting 5 m below the highstand watermark of the Yamula reservoir on the Kızılırmak River near Taşhan village. The section starts with an alternation of cross-bedded siltstones and sandstones that are in places calcareous and include gravels of ophiolitic cherts, followed by an alternation of claystones and dominantly (massive, clayey or nodular) limestones that are covered by an ignimbrite. The ignimbrite (25.5–37.0 m) was dated at 7.51 ± 0.07 Ma and 7.52

± 0.14 Ma ($^{40}Ar/^{39}Ar$, amphibole and plagioclase, respectively; Meijers et al., 2018b). The top of the ignimbrite is reworked into overlying coarse fluvial sediments. Above an unexposed interval, the top of the section (71–96 m) starts with a cross-bedded conglomerate that contains angular chert and mud-ball pebbles, followed by unconsolidated sands and massive red clays, and eventually (massive, nodular) carbonates, which are in places dolomitic and crumbly or nodular. The overlying 120 m of the sediment succession was not sampled and is overlain by a basalt flow, which is in turn separated by an erosional unconformity from the overlying Valibabatepe ignimbrite (2.52 ± 0.49 Ma and 2.73 ± 0.08 Ma, both $^{40}Ar/^{39}Ar$; Aydar et al., 2012; Higgins et al., 2015).

The 35 $\delta^{13}C$ and $\delta^{18}O$ values average –0.6‰ ± 2.0‰ and 22.3‰ ± 0.5‰, respectively. The $\delta^{13}C$ values tend to be higher in the upper, dominantly limestone portion of the section. No trend can be observed in the $\delta^{18}O$ values.

Protracted Sedimentation in Intramontane Mio-Pliocene Basins

The sampled sections belong to a series of depocenters that have been only moderately incised since sediment deposition ceased, such that the overall thickness of exposed sediment is potentially limited compared to the total sediment thickness. Most sections were sampled (nearly) to the top of sedimentary exposure (except for sections TS and HA), whereas the deepest sedimentary rocks filling each basin were typically not accessible (with the exception of section IB-KAR). Therefore, our results only document isotopic trends toward the end of sedimentation in each of the depocenters.

The time intervals captured within the sampled sections individually span ~0.2–2.5 m.y. Age constraints are most robust within sections with $^{40}Ar/^{39}Ar$ ages from multiple levels (the GU section covers ~2.5 m.y.) and by the KU section which was dated using magnetostratigraphy. The latter constrains the duration of sedimentation of the sampled KU section to ~1.8 m.y. A compilation of well-dated Neogene Anatolian fluvio-lacustrine sections yields an average sedimentation rate of 7.5 cm/k.y. for Oligocene to Miocene Anatolian continental basins (Meijers et al., 2018b). According to this rate, the shortest section (IB-KAR, 17.7 m) still covers a time interval of >200 k.y.

DISCUSSION

Hydrology and Extent of Sedimentation of the Central Anatolian Lake System

Open and Closed Lake Hydrology

Changes in lake carbonate $\delta^{13}C$ values generally result from changes in biogenic productivity (e.g., Li and Ku, 1997). Because ^{12}C is preferentially partitioned into lake organic matter, an increase in biogenic productivity results in a relative increase of ^{13}C in dissolved CO_2, which is taken up by carbonates that precipitate from lake water. Therefore, an increase in $\delta^{13}C$ values generally reflects an increase in lake productivity. Further, an increase in evaporation generates higher $\delta^{18}O$ values, because ^{16}O is preferentially removed from the lake water during evaporation.

Based on information about the sediment and water supply (which is linked to precipitation and evaporation) as well as the potential accommodation space (which is linked to subsidence) of a lake, Carroll and Bohacs (1999) designed a lake basin classification. The tripartite lake basin classification categorizes lakes as either overfilled, balanced fill, or underfilled. From a stable isotope perspective, lake hydrology can be categorized as open or closed. The former refers to lakes that maintain a stable water level, which is controlled by a surface outlet. Conversely, a closed lake is characterized by limited surface or underground outflow, meaning that most water exits the lake through evaporation. Under such circumstances, lake levels respond to fluctuations in the amount of riverine input and evaporation. A closed lake hydrology is indicated by a positive covariance between $\delta^{13}C$ and $\delta^{18}O$, when evaporation and lake productivity are generally governed by changes in temperature during carbonate formation. A hydrologically closed lake corresponds to an underfilled lake in the classification of Carroll and Bohacs (1999). Hydrologically open lakes correspond to balanced fill and overfilled lakes.

Data from five sections exhibit a significant positive covariance between $\delta^{13}C$ and $\delta^{18}O$ values, which points to closed lake hydrology: sections GU, IB-KAR, HC, KU, and the lower part of KZK (Figs. 4, 6; Table S1 [footnote 1]). Within the data sets from the remaining sections, we observe either no covariance between $\delta^{13}C$ and $\delta^{18}O$ (sections BH, TS, BO) or a negative covariance (sections GO, OV, BK, AZ, HA, and the upper part of KZK; Figs. 4, 6; Table S1), which indicates open lake hydrology. Open as well as closed lake conditions are observed rather randomly across the study region, irrespective of their age or location. We hence do not discern any spatiotemporal trend across our regional data set.

Time Span and Paleogeographic Setting of Each Section

Akmezar (AZ). The lower part (0–20 m) of the Akmezar section consists of the Göbü tuff (6.5 ± 0.3 Ma; Meijers et al., 2018b). The section is covered by the ca. 2.6 Ma Valibabatepe ignimbrite (above 102 m; Aydar et al., 2012; Higgins et al., 2015), atop an unexposed interval between 93.5 and 102 m. Where exposed in the vicinity of the section, the sole of the ignimbrite overlies thermally heated evolved paleosols, which indicates a time gap between deposition of the topmost part of the section and the emplacement of the ignimbrite. The ignimbrite forms a regionally extensive mesa, which has been incised by the Zamantı River. The section spans the entire thickness of underlying sediments that were exposed by river incision along the river valley. Ignimbrite occurrences on the valley floor ~30 km farther downstream the Zamantı River show that the valley had already been incised close to its current depth when the ignimbrite was emplaced and draped the valley and its surrounding terraces (Fig. S2 [footnote 1]). Based on a number of sections with multiple age constraints, the estimated average sedimentation rate in central Anatolia is 7.5 cm/k.y. (Meijers et al., 2018b). The youngest sedimentary

rocks at the top of the Akmezar section are therefore estimated to be ca. 5.3 Ma. The estimated time gap of 2.7 m.y. between the youngest sedimentary rocks at top of the section and ignimbrite emplacement therefore brackets the time span (5.3–2.6 m.y.) during which incision of the Zamantı River started.

Bayramhacı (BH). The convolute bedding at ~13 m and between 30 and 42 m (Figs. 7B, 7C) was produced on a flat-lying lake bed and resembles structures produced by ground shaking (seismites). We interpret the slumped interval between 46 m and 92 m (Figs. 2, 7A), however, as deformation resulting from the emplacement of the ignimbrite onto the soft lake sediments. The large-scale convolute bedding may be the result of rapid gravity-driven sediment mobilization during the emplacement of the massive pumiceous ignimbrite.

Based on the age of the ash layer near the base of the section (9.96 ± 0.08 Ma, $^{40}Ar/^{39}Ar$ on biotite; Meijers et al., 2018b), the regional sedimentation rate of 7.5 cm/k.y. (Meijers et al., 2018b), and assuming that the slumped interval (46–92 m) was deposited instantaneously, the 130-m-thick section most likely covers the time interval from 10.1 to 9.0 Ma. The large pumiceous ignimbrite occurring 35 m above the dated ash layer within the section is most likely the Kavak or Zelve ignimbrite. The most recent ages obtained for the Kavak ignimbrite range from 10.5 to 9.1 Ma, and for the Zelve ignimbrite, 9.9–9.1 Ma (Lepetit et al., 2014; Aydar et al., 2012). Given the proposed spatial extent of the Kavak and Zelve ignimbrites (Le Pennec et al., 1994), the ignimbrite within the Bayramhacı section is most likely the Zelve ignimbrite.

Boğazlıyan (BO). The Boğazlıyan section comprises the topmost beds of a much thicker succession that contains two interbedded ignimbrites of 6.81 ± 0.24 Ma and 5.02 ± 0.20 Ma (Özsayın et al., 2013). If we assume that the sedimentation rate after the deposition of the second ignimbrite did not change compared to the 8.0 cm/k.y. sedimentation rate between the two ignimbrites, we find that the Kışladağ Limestone Member at the top of the section was deposited ca. 3.7 Ma.

The sedimentary rocks of the Boğazlıyan section were deposited over the footwall of the Tuz Gölü fault, which presently acts as a normal fault under a NE-SW extensional regime (Kürçer and Gökten, 2012; Özsayın et al., 2013; Yıldırım, 2014). Prior to 6.8 Ma, and possibly until the Pliocene, the fault acted as a strike-slip fault with a minor reverse component (Özsayin et al., 2013). Changeover from a compressional to an extensional stress regime of the Tuz Gölü fault occurred by the start of the Pliocene (Özsayin et al., 2013). The sedimentary rocks of the BO section are perched ~400 m above the actively aggrading basin floor of the Tuz Gölü Basin in the hanging wall of the fault. The 400 m represents the minimum vertical separation across the fault since deposition of section BO. Sedimentary rocks exposed at section BO indicate a low-energy depositional environment, and therefore the Tuz Gölü fault was unlikely to have had a surface expression during deposition of the sediments.

Büyükkünye (BK). The Büyükkünye section consists of two subsections (Fig. S1 [footnote 1]) juxtaposed across an unexposed erosive or tectonic contact. One subsection, which we interpret to be in a lower stratigraphic position, contains clastic sedimentary rocks, paleosols, and a 5.6 Ma pumiceous ash layer (Meijers et al., 2018b). The other subsection consists entirely of lacustrine limestones with travertine intervals. The rock types of the lower subsection indicate sedimentation under high- to low-energy fluvial depositional conditions, allowing for the preservation of the tuff layer, with intermittent periods of ceased sedimentation that allowed for soil formation. The limestone beds of the upper subsection indicate carbonate precipitation under persistent lacustrine conditions, with little evidence for nondepositional intervals, and little clastic input. The unexposed contact between the two sections may be the steep flank of a paleovalley incised in the sediments of the clastic section, or a steeply dipping fault with a normal component with the clastic section in the footwall. The former explanation seems less likely, given that it would be very difficult to maintain a steep paleovalley in soft clastic sediments during deposition adjacent to lacustrine carbonate without any downslope transport and dispersal of clastic sediment into the carbonates. We therefore assume that the two subsections were offset by a fault after deposition. A minimum age for both sections is provided by the ca. 2.6 Ma Valibabatepe ignimbrite (Aydar et al., 2012; Higgins et al., 2015), which caps the hill that exposes the two subsections. In the surrounding region, the ignimbrite flowed across an already differentiated landscape of flat-lying, unincised former Pliocene sediment depositional surfaces, as well as already deeply incised narrow stream valleys (see, e.g., Fig. S2 [footnote 1]). However, the areal extent of the dissected landscape was not as extensive as today. By analogy to section AZ, the end of fluvio-lacustrine sedimentation was likely followed by several million years of nondeposition prior to the emplacement of the Valibabatepe ignimbrite.

Gürün (GU). Unlike sections from other basins presented in this study, the Gürün Basin was affected by substantial post-depositional folding (Önal et al., 2004). In its lower part, the GU section yields the highest $\delta^{18}O$ values of all sampled sections. The positive covariance between $\delta^{13}C$ and $\delta^{18}O$ indicates closed lake conditions. Across the basalt that separates the lower and upper sampled lacustrine sequence, a large decrease of 6‰–7‰ occurs in both $\delta^{13}C$ and $\delta^{18}O$ values. The lower $\delta^{18}O$ and $\delta^{13}C$ values in the upper part of the section are indicative of a more positive water balance alongside a decrease in biogenic productivity. Given that the isotopic shift in both carbon and oxygen directly followed lava emplacement, we conclude that the flow likely modified the lake's volume and/or dimensions. The change in isotopic composition can therefore be explained not by climatic factors, but rather by modifications to lake connectivity and openness.

Spore and pollen fossils of the Çayboyu Member of the Gürün Formation indicate that the Gürün Basin fill is of middle Miocene age (Önal et al., 2004). However, $^{40}Ar/^{39}Ar$ chronology (three whole-rock ages, Burdigalian; Meijers et al., 2018b) of the younger Terzioğlu Member indicates that the basin is older, and of early Miocene age. The GU section is therefore the only section that is not late Miocene to Pliocene in age.

Güzelöz (GO). Published stable isotope geochemistry results from the Güzelöz section (six samples; Göz et al., 2014) fall within the range of the $\delta^{13}C$ and $\delta^{18}O$ values presented here. Assuming that sedimentation at section GO occurred with an average regional sedimentation rate of 7.5 cm/k.y.

(Meijers et al., 2018b), sedimentation at section GO would have continued well into the Pliocene (until ca. 3.5 Ma), therefore likely making it one of the youngest sampled sections.

Hacıbekirli (HC). The beds of the Hacıbekirli section slant slightly to the northwest (302°/12°, dip direction and dip angle). The sequence forms part of the northern limb of the Tauride Mountains antiformal arch (Radwany et al., 2017). Final sedimentation at section HC is estimated to have occurred at ca. 5.7 Ma, based on an average regional sedimentation rate of 7.5 cm/k.y. (Meijers et al., 2018b). In the absence of detectable fanning of bedding dip at the scale of the outcrop, it appears that any syndepositional tilting over the duration of deposition of the measured section is small compared to the finite amount of post-depositional tilting. This means that the distal northern limb of the Tauride arch continued to develop after ca. 5.7 Ma, through broadening and/or amplification.

Haliminhanı (HA). The age of the Haliminhanı section is constrained to 8.9–7.4/6.8 Ma (Hilgen et al., 2012) by mammal stratigraphy, which indicates an MN11–MN12 age (e.g., The NOW Community, 2017; Kaya and Kaymakçı, 2013). Atop the sampled stable isotope section, another 160 m of unsampled stratigraphy is exposed, and terminates with the deposition of less-clastic lacustrine carbonates. If deposition continued at the regional rate of 7.5 cm/k.y. (Meijers et al., 2018b), fluvio-lacustrine sedimentation in this part of the Sivas Basin would have continued for another 2.1 m.y., thereby possibly continuing into the Pliocene.

Ibrala (IB-KAR). The Ibrala section is the only section where fluvial and lacustrine rocks directly and conformably overlie nearshore and estuarine marine rocks. The Serravallian age (13.82–11.62 Ma; Ćorić et al., 2012; Hilgen et al., 2012) of the marine rocks therefore marks the switch from marine to continental sedimentation in the southwestern portion of the CAP (see also Meijers et al., 2018b).

Kozaklı (KZK). $\delta^{13}C$ and $\delta^{18}O$ values in the Kozaklı section change from positive covariance to negative covariance upsection, thereby indicating a shift from closed to open lake conditions. Paleolake Kozaklı is the sole Anatolian lake within our study that displays this shift. The ignimbrite at the base of the section was dated at 7.6 ± 0.5 Ma (Meijers et al., 2018b). Using an average sedimentation rate of 7.5 cm/k.y. (Meijers et al., 2018b), the change in lake hydrology occurred at ca. 7.4 Ma. Assuming the same rate, fluvio-lacustrine sedimentation at Kozaklı may have continued until ca. 6.8 Ma.

Kumarlı (KU). Magnetostratigraphy and an $^{40}Ar/^{39}Ar$ age from the top of the section indicate that fluvio-lacustrine sedimentation in the Kangal Basin must have ceased by ca. 4.8 Ma (Meijers et al., 2018a).

Özvatan (OV). The (upper Miocene–)lower Pliocene lacustrine carbonates of the Özvatan section are interfingered with alluvial fan deposits that are derived from higher-elevation areas of the Central Anatolian Crystalline Complex (Fig. S3 [footnote 1]). Initially restricted to the basin sides, the alluvial fan deposits must have prograded across the lacustrine domain, thereby depositing a thin, extensive layer of clastic sediments over the lacustrine unit.

Taşhan (TS). Similar to the HA section, the Taşhan section continues above the sampled interval for another ~100–140 m (2–3 km southwest of section TS) and is capped by a basalt. Using the regional 7.5 cm/k.y. sedimentation rate (Meijers et al., 2018b), sedimentation possibly continued until ca. 5.4–4.9 Ma. The Valibabatepe ignimbrite (ca. 2.6 Ma; Aydar et al., 2012; Higgins et al., 2015) unconformably covers the top of the section, which suggests a significant amount of time between final fluvio-lacustrine sedimentation and ignimbrite emplacement.

Origin of Limestone-Forming Events during Final Fluvio-Lacustrine Sedimentation

In spite of a great variety of rock types and fluctuating depositional environments, sedimentation in the investigated sections almost invariably finishes under limestone-forming lacustrine conditions (Fig. 3). All sections sampled in upper Miocene–Pliocene rocks (except for section TS) display a terminal phase of limestone deposition just before sedimentation ceased and incision began.

It would be difficult to hold climate change responsible for the final phase of lacustrine limestone deposition, because the onset of final lacustrine sedimentation occurred asynchronously over the various sampled basins (Figs. 3, 4). Alternatively, because limestones form protective caps that prevent the erosion of underlying layers, the systematic termination of sedimentation with the deposition of relatively resistant layers could be regarded as preservation bias. In such a case, any clastic layer deposited after limestone deposition would have been eroded away. This scenario is highly unlikely, however, because (1) the contrast in erodibility between clastic and limestone layers is not sufficient for erosion to perfectly strip off a soft cover without incising the limestones and leaving residual patches of the overlying cover along drainage divides, and (2) thin, continuous clastic levels of at most a few meters thick are locally found between the cap carbonates and overlying ignimbrites. Therefore, we regard the trend of final limestone deposition within most basins as a true, diachronous signal, independent of climate change. We argue that the process leading to the cessation of sedimentation in the intramontane basins is also responsible for the deposition of the cap carbonates.

Extent and Connectivity of the Lakes Based on the Stable Isotopic Record

Although the sections are widely distributed throughout the study area, some lie in close proximity and their depositional ages overlap. Deposition, therefore, may have occurred within the same lake. The size, shape, and extent of the lakes are difficult to constrain. It is unclear whether the cap carbonate mesas of the present-day CAP are the scarce remnants of much wider lakes, or the well-preserved remnants of much smaller lakes, for which evidence may be qualitatively deduced from the age constraints in Figure 4. Additionally, because the upper Miocene to Pliocene lakes occupied inward-draining basins, their size and extent probably fluctuated rapidly and widely in response to changes in water balance. One way to test whether separate sections of similar age belong to a single lake is to compare their isotopic record, and to test whether they share similarities in $\delta^{18}O$ and $\delta^{13}C$ values and covariance.

While similarities are a strong argument for sedimentation within a common lake, the reverse is not true, as wide, shallow lakes can maintain perennial spatial variations in average annual $\delta^{18}O$ values (Shi et al., 2017; Wen et al., 2016). While inconclusive, a discussion on the extent and connectivity of the former lakes can be found in the Supplemental Material (File S1 [footnote 1]).

Factors Controlling the Evolution of the Mio-Pliocene Central Anatolian Lakes

Paleoenvironmental Conditions during the Late Miocene to Pliocene Rise of the CAP and its Margins

The sampled former depocenters evolved during the rise of the Anatolian plateau and its northern and southern margins (Yıldırım et al., 2011; Meijers et al., 2018b) between 11 and 5 Ma (Cosentino et al., 2012; Meijers et al., 2018b). The rise of the CAP and its southern margin is expressed by a 3‰–4‰ decrease of the lowest 25% of $\delta^{18}O$ values of the lacustrine carbonates, interpreted to reflect a similar decrease in $\delta^{18}O$ of precipitation as a result of plateau uplift (Meijers et al., 2018b). Paleoprecipitation estimates based on the coexistence approach indicate MAPs of 1000–1400 mm from the late early Miocene to the Pliocene, with a period of lower values of ~900 mm during the late to latest Miocene (Kayseri-Özer, 2017). The paleoprecipitation estimates therefore indicate a (sub)humid Anatolian climate during late Miocene surface uplift. Eventually, the rise of the Tauride and Pontide Mountains generated a rain shadow, which led to semiarid conditions within the plateau interior that contrast with the humid conditions observed along the Mediterranean and Black Sea coasts. The present-day rain shadow is expressed by low $\delta^{18}O$ values of surface waters along the immediate leeward flanks of both mountain belts; higher $\delta^{18}O$ values in the plateau interior result from evaporation (Schemmel et al., 2013). Today, the remaining lakes of the CAP experience highly evaporative conditions, resulting in $\delta^{18}O$ values of lacustrine carbonate of up to 36‰ in close-to-modern lake carbonates (late Pleistocene to Holocene; e.g., Leng et al., 1999; Roberts et al., 2001; Jones et al., 2006, 2007; Dean et al., 2015).

The $\delta^{13}C$ and $\delta^{18}O$ values obtained from the former depocenters show little variability in a number of cases (as expressed by standard deviations ≤1.1‰ for sections KU and OV and the lower part of section BK), and individual records display no significant trend toward higher or lower values with time (sections KU and OV and the lower parts of sections BK, as well as sections AZ, BH, HA, TS), in spite of coeval changes in sediment composition. We therefore conclude that lake hydrology was relatively stable over extended periods of time: ~1.8 m.y. for section KU, and arguably >1.0 m.y. for section HA. Such stability is remarkable, given that the studied basins evolved during a tectonically active period, namely the formation of the CAP and its southern and northern margins. Additionally, no increasingly evaporative trend (as expressed in modern lake $\delta^{18}O$ values >36‰) is observed within the Miocene to early Pliocene lake carbonates during surface uplift of the CAP and its southern margin, which one would expect during the formation of a rain shadow. The highest $\delta^{18}O$ values of up to 35‰ occur within the oldest sampled carbonates (ca. 20–17.5 Ma, section GU; Figs. 4, 5). During surface uplift (11–5 Ma), only carbonates at the top of section HC (ca. 6 Ma) range up to 33‰. Besides one $\delta^{18}O$ value of ~28‰ within section BO, all other $\delta^{18}O$ values reported here, as well as within the previously published ca. 10 Ma Tuğla section (Çankırı Basin; Fig. 1C; Mazzini et al., 2013), remain <27‰. Late Miocene surface uplift therefore seemingly did not generate intense aridification of the CAP interior during the late Miocene to early Pliocene, although this is a trend that may be obscured in hydrologically open lakes (Fig. 4) where through-flowing waters could counter an aridification trend.

We explain the absence of an aridification trend (i.e., a temporal trend toward higher $\delta^{18}O$ values in the sampled sections) by the relatively humid climate of Miocene to Pliocene Anatolia. Under humid conditions, the water balance of the lakes during carbonate precipitation could have continued to remain positive, thereby explaining the absence of $\delta^{18}O$ values indicative of high evaporation. Similarly, the absence of an aridification trend by the time of the full establishment of a Tauride Mountains orographic barrier at 5 Ma may be explained by the counteracting increase in MAP into the Pliocene (Kayseri-Özer, 2017).

Summer drought has been recorded on the Iberian Peninsula since the late Pliocene (ca. 3.4 Ma; Jiménez-Moreno et al., 2010). Similarly, grassland expansion in Anatolia since the late Miocene (Akgün et al., 2007; Strömberg et al., 2007) may not have led to pronounced seasonality in the eastern Mediterranean until the late Pliocene. In concert with high MAP, reduced seasonality in Anatolia during late Miocene to Pliocene surface uplift may have allowed year-round delivery of moisture to the Anatolian lake system and the absence of an aridification trend in lake records.

The Çankırı Basin at the northern end of the CAP interior seems to be an important exception in terms of absence of aridification. Here, hypersaline lake conditions resulted in the deposition of evaporites within vast areas during the late Miocene and early Pliocene (Karadenizli, 2011; Mazzini et al., 2013), thereby clearly marking (semi)arid conditions.

An environmental event that could have affected the climate of the CAP is the Messinian Salinity Crisis (MSC). During the MSC, dramatic climatic changes occurred within the Mediterranean and Paratethys basins as a result of restricted connectivity of these basins with the Atlantic Ocean. The $\delta^{13}C$ and $\delta^{18}O$ values of section KU, however, indicate that the MSC did not cause significant changes in the hydrology of lake Kangal (Meijers et al., 2018a).

Chronology of the Expansion and Demise of the Mio-Pliocene Continental Depocenters

A compilation of the youngest marine sedimentary rocks (Meijers et al., 2018b) reveals that the switch to nonmarine sedimentation likely occurred at ca. 12–11 Ma in the southern portion of the CAP (compare the ca. 13 Ma and ca. 8 Ma paleogeographic sketches in Figs. 2A, 2B). This provides a maximum age for the onset of lacustrine sedimentation in the continental basins that have since covered much of the CAP. Paleogeographic

information (Figs. 2A, 2B) suggests that the Anatolian lake system expanded during surface uplift of the CAP interior.

Lacustrine sedimentation in the southeastern CAP ended at or around the Miocene-Pliocene boundary (ca. 5 Ma; Fig. 4), with the exception of sections BO and GO, where sedimentation continued until ca. 3.7 Ma and ca. 3.5 Ma, respectively (Zanclean-Piacenzian boundary, i.e., the early to late Pliocene boundary). Sedimentation in the northern CAP (Çankırı Basin; Fig. 1C) also continued until ca. 3.6 Ma (Kayseri-Özer, 2017), whereas sedimentation within a few large depocenters in the present-day Konya closed catchment area likely continued well into the late Pliocene to Pleistocene and even up to the present day in its northern portion (lake Tuz Gölü; Figs. 1A, 1C; see, e.g., Fernandez-Blanco et al., 2013). In summary, lacustrine sedimentation ceased between the late Miocene and early Pliocene east of the Tuz Gölü fault (Figs. 1A, 1C), while it continued west of the fault. Former depocenters of the eastern CAP are now incised by rivers that drain toward the Mediterranean Sea, the Black Sea, and the Persian Gulf.

The Demise of the Central Anatolian Lakes

In the late Miocene–early Pliocene, numerous lakes occupied the CAP. According to the carbonate isotope record, most lakes were hydrologically open, with the exception of two lakes (Fig. 4) located near the southern margin of the plateau, as well as in the Çankırı Basin near the northern margin of the plateau (ca. 10 Ma; Fig. 1C; Mazzini et al., 2013). Of the two closed lakes (sections HC and KU) within the plateau interior, one former lake (section HC) is presently located within the Konya closed catchment. The open lakes drained either to the surrounding seas or to terminal lakes within the plateau interior.

Incision of the lake outlets remained limited, allowing lacustrine sedimentation under open lake conditions over more than a million years in most basins. Lake Kozaklı is the only lake that experienced a switch from closed to open hydrology at ca. 7.5 Ma. Inception of overflow at the time did not lead to any substantial incision of the outlet, allowing for the lake to exist for an additional ~700 k.y. First, limited outlet incision requires very low topographic gradients within the plateau interior. Second, if the lakes drained to the surrounding seas, then the steepening of the plateau margins resulting from plateau uplift would have resulted in the incision of the plateau margin drainage and the progressive propagation of incision upstream toward the plateau interior. The fluvio-lacustrine basins of the plateau interior would eventually have been dissected and the lakes would have drained away. It is therefore likely that the open lakes instead drained into a single or multiple terminal lakes, such as Lake Kangal, thereby maintaining a high base level within the plateau interior.

Yet, between ca. 5 Ma and ca. 3.6 Ma (i.e., during the early Pliocene), most of the lakes in the eastern CAP drained away and their floors were incised (Figs. 2C, 4). If a major shift from closed lakes to open lakes was observed at the time, one could argue that lake overflow would have been the cause of drainage integration across the plateau interior and their subsequent incision. Yet, open lake conditions persisted for long periods of time.

The establishment of connections between the internal drainage and the surrounding seas, in particular the Mediterranean Sea after 5.5 Ma, as evidenced by provenance studies in the Adana Basin (Fig. 1C; Radeff et al., 2017), and possibly over the same period with the Persian Gulf and Black Sea, would have allowed for incision to propagate into the plateau interior, thereby ending lacustrine conditions in the southeastern CAP after the Miocene (Fig. 2C). The Zamantı River, a tributary of the Seyhan River that drains the southeastern CAP, would have then started reaching the Mediterranean coast in the Adana Basin at 5.5 Ma. Incision would have propagated upstream along the Zamantı River and its tributaries, thereby reaching section AZ at 5.3 Ma and section BK at 4.9 Ma. Some 10–30 km downstream of these sections, the Zamantı River had already reached its current depth of incision by the time of deposition of the ca. 2.6 Ma Valibabatepe ignimbrite.

Sedimentation east of the Tuz Gölü fault likely ended (ca. 3.7 Ma, section BO) slightly before sedimentation in the Çankırı Basin (at ca. 3.6 Ma), when the Kızılırmak River led to the incision of sediment fills of the former depocenters in both areas. Their incision marked the end of the late Miocene to early Pliocene phase of drainage integration and lake disappearance. Since the early Pliocene, little has changed in the drainage system of the southern CAP, when it was composed of an internally draining Konya closed catchment in the west and a dissected plateau in the east.

The combination of established chronologies with sedimentological characterization and stable isotope analyses for 13 basins in the southern CAP reveals important clues about the development of the Anatolian lake system during the late Miocene to Pliocene. Fluvio-lacustrine sedimentation of substantial duration occurred under fairly constant environmental and climatic conditions, during a time of the formation of the Anatolian microplate, surface uplift of the CAP and its northern and southern margins, and an overall change from a compressional to an extensional geodynamic setting.

CONCLUSIONS

(1) Open lake hydrology persisted in the fluvio-lacustrine basins of the Central Anatolian Plateau interior during surface uplift of the plateau. Surface uplift did not result in coeval incision of these basins, as one would expected as a result of an increase in the topographic gradient between the plateau interior and its margins. This suggests that the plateau interior was disconnected from marine basins and occupied by inward-draining lakes.

(2) Inverse covariance of $\delta^{13}C$ and $\delta^{18}O$ from eight sections suggest that basin-capping lacustrine carbonates were deposited in open lakes, with the exception of four sections located along the northern flank of the Tauride Mountains, where positive $\delta^{13}C$ and $\delta^{18}O$ covariance suggests deposition in closed lakes. Data from one section display a hydrological switch from closed to open lake conditions.

(3) Consequently, the hydrologically open lakes were likely draining into terminal lakes, such as paleolake Kangal, or various paleolakes occupying the present-day Konya closed catchment.

(4) The $\delta^{13}C$ and $\delta^{18}O$ values from 13 Miocene to Pliocene fluvio-lacustrine sections indicate slow changes in environmental conditions during lake basin sedimentation that occurred during surface uplift of the Central Anatolian Plateau.

(5) The $\delta^{18}O$ data do not yield increasingly high values with time, which indicates the absence of major aridification during the early phases of surface uplift of the Central Anatolian Plateau and its margins. This may have been caused by prominent westerly storm tracks permitting moisture transport onto the evolving plateau. Minor aridification may also be obscured in our data set by an overall wet subtropical climate with adequate moisture availability and a reduced seasonality.

(6) The onset of river incision roughly coincides with a switch from contractional to extensional deformation in central Anatolia. Compression may have led to the creation of new, tectonically induced relief across the subdued topography of the plateau interior, thereby generating a new partitioning of the depocenters, which modified the water balance and promoted drainage integration across the eastern Central Anatolian Plateau.

(7) The last continental sedimentation was of lacustrine nature (i.e., carbonates, marls) in most of the sampled basins. Given that final sedimentation occurred at different times, it is unlikely that climatic drivers were responsible for final lacustrine sedimentation.

ACKNOWLEDGMENTS

The authors acknowledge support through the U.S. National Science Foundation Continental Dynamics (CD) program (EAR-1109762, "Central Anatolian Tectonics [CD-CAT]" to Whitney); Côme Lefebvre, Tamás Mikes, Ahmet Peynircioğlu, Seçkin Şiş, Levent Tosun, and Jane Willenbring are thanked for field assistance; and Jens Fiebig is thanked for laboratory support at the joint Goethe University–Senckenberg BiK-F Stable Isotope Facility. We would like to thank Faruk Ocakoğlu and Joel Saylor for constructive and helpful reviews.

REFERENCES CITED

Akgün, F., Kayseri, M.S., and Akkiraz, M.S., 2007, Paleoclimatic evolution and vegetational changes during the Late Oligocene–Miocene period in Western and Central Anatolia (Turkey): Palaeogeography, Palaeoclimatology, Palaeoecology, v. 253, p. 56–90, https://doi.org/10.1016/j.palaeo.2007.03.034.

Aydar, E., Schmitt, A.K., Çubukçu, H.E., Akin, L., Ersoy, O., Sen, E., Duncan, R.A., and Atici, G., 2012, Correlation of ignimbrites in the central Anatolian volcanic province using zircon and plagioclase ages and zircon compositions: Journal of Volcanology and Geothermal Research, v. 213, p. 83–97, https://doi.org/10.1016/j.jvolgeores.2011.11.005.

Bassant, P., Van Buchem, F.S.P., Strasser, A., and Görür, N., 2005, The stratigraphic architecture and evolution of the Burdigalian carbonate–siliciclastic sedimentary systems of the Mut Basin, Turkey: Sedimentary Geology, v. 173, p. 187–232, https://doi.org/10.1016/j.sedgeo.2004.01.017.

Carroll, A.R., and Bohacs, K.M., 1999, Stratigraphic classification of ancient lakes: Balancing tectonic and climatic controls: Geology, v. 27, p. 99–102, https://doi.org/10.1130/0091-7613(1999)027<0099:SCOALB>2.3.CO;2.

Ćorić, S., Harzhauzer, M., Rögl, F., İslamoğlu, Y., and Landau, B., 2012, Biostratigraphy of some mollusc-bearing middle Miocene localities on the Karaman high plain (Turkey, Konya Province): Cainozoic Research, v. 9, p. 281–288.

Cosentino, D., Schildgen, T.F., Cipollari, P., Faranda, C., Gliozzi, E., Hudáčková, N., Lucifora, S., and Strecker, M.R., 2012, Late Miocene surface uplift of the southern margin of the Central Anatolian Plateau, Central Taurides, Turkey: Geological Society of America Bulletin, v. 124, p. 133–145, https://doi.org/10.1130/B30466.1.

Dean, J.R., Jones, M.D., Leng, M.J., Sloane, H.J., Roberts, C.N., Woodbridge, J., Swann, G.E., Metcalfe, S.E., Eastwood, W.J., and Yiğitbaşıoğlu, H., 2013, Palaeo-seasonality of the last two millennia reconstructed from the oxygen isotope composition of carbonates and diatom silica from Nar Gölü, central Turkey: Quaternary Science Reviews, v. 66, p. 35–44, https://doi.org/10.1016/j.quascirev.2012.07.014.

Dean, J.R., Jones, M.D., Leng, M.J., Noble, S.R., Metcalfe, S.E., Sloane, H.J., Sahy, D., Eastwood, W.J., and Roberts, C.N., 2015, Eastern Mediterranean hydroclimate over the late glacial and Holocene, reconstructed from the sediments of Nar lake, central Turkey, using stable isotopes and carbonate mineralogy: Quaternary Science Reviews, v. 124, p. 162–174, https://doi.org/10.1016/j.quascirev.2015.07.023.

Demirtaşlı, E., Turhan, N., Bilgin, A.Z., and Selim, M., 1984, Geology of the Bolkar mountains, *in* Tekeli, O., and Göncüoğlü, M.C., eds., Geology of the Taurus Belt: International Symposium, Mineral Research and Exploration Institute, Ankara, 26–29 September 1983: Ankara, Geological Society of Turkey and the Mineral Research and Exploration Institute, p. 125–141.

Denk, T., Zohner, C.M., Grimm, G.W. and Renner, S.S., 2018, Plant fossils reveal major biomes occupied by the late Miocene Old-World Pikermian fauna: Nature Ecology & Evolution, v. 2, 1864, https://doi.org/10.1038/s41559-018-0695-z.

Eriş, K.K., Bassant, P., and Ülgen, U.B., 2005, Tectono-stratigraphic evolution of an Early Miocene incised valley-fill (Derinçay Formation) in the Mut Basin, Southern Turkey: Sedimentary Geology, v. 173, p. 151–185, https://doi.org/10.1016/j.sedgeo.2003.12.011.

Fernández-Blanco, D., Bertotti, G., and Çiner, A., 2013, Cenozoic tectonics of the Tuz Gölü Basin (Central Anatolian Plateau, Turkey): Turkish Journal of Earth Sciences, v. 22, p. 715–738, https://doi.org/10.3906/yer-1206-7.

Göz, E., Kadir, S., Gürel, A., and Eren, M., 2014, Geology, mineralogy, geochemistry, and depositional environment of a Late Miocene/Pliocene fluviolacustrine succession, Cappadocian Volcanic Province, central Anatolia, Turkey: Turkish Journal of Earth Sciences, v. 23, p. 356–411, https://doi.org/10.3906/yer-1307-17.

Gürsoy, H., Tatar, O., Piper, J.D.A., Koçbulut, F., Akpınar, Z., Huang, B., Roberts, A.P., and Mesci, B.L., 2011, Palaeomagnetic study of the Kepezdağ and Yamadağ volcanic complexes, central Turkey: Neogene tectonic escape and block definition in the central-east Anatolides: Journal of Geodynamics, v. 51, p. 308–326, https://doi.org/10.1016/j.jog.2010.07.004.

Higgins, M., Schoenbohm, L.M., Brocard, G., Kaymakçı, N., Gosse, J.C., and Cosca, M.A., 2015, New kinematic and geochronologic evidence for the Quaternary evolution of the Central Anatolian fault zone (CAFZ): Tectonics, v. 34, p. 2118–2141, https://doi.org/10.1002/2015TC003864.

Hilgen, F.J., Lourens, L.J., Van Dam, J.A., Beu, A.G., Boyes, A.F., Cooper, R.A., Krijgsman, W., Ogg, J.G., Piller W.E., and Wilson, D.S., 2012. The Neogene Period, *in* Gradstein, F.M., Ogg, J.G., Schmitz, M.D., and Ogg, G.M., eds., The Geologic Time Scale: Boston, Elsevier, p. 923–978, https://doi.org/10.1016/B978-0-444-59425-9.00029-9.

Huang, S., Meijers, M.J.M., Eyres, A., Mulch, A., and Fritz, S.A., 2019, Unravelling the history of biodiversity in mountain ranges through integrating geology and biogeography: Journal of Biogeography, v. 46, p. 1777–1791, https://doi.org/10.1111/jbi.13622.

Jaffey, N., and Robertson, A.H.F., 2001, New sedimentological and structural data from the Ecemiş Fault Zone, southern Turkey: Implications for its timing and offset and the Cenozoic tectonic escape of Anatolia: Journal of the Geological Society, v. 158, p. 367–378, https://doi.org/10.1144/jgs.158.2.367.

Jaffey, N., and Robertson, A., 2005, Non-marine sedimentation associated with Oligocene-Recent exhumation and uplift of the Central Taurus Mountains, S Turkey: Sedimentary Geology, v. 173, p. 53–89, https://doi.org/10.1016/j.sedgeo.2003.11.025.

Jiménez-Moreno, G., Fauquette, S., and Suc, J.-P., 2010, Miocene to Pliocene vegetation reconstruction and climate estimates in the Iberian Peninsula from pollen data: Review of Palaeobotany and Palynology, v. 162, p. 403–415, https://doi.org/10.1016/j.revpalbo.2009.08.001.

Jones, M.D., Roberts, C.N., Leng, M.J., and Türkeş, M., 2006, A high-resolution late Holocene lake isotope record from Turkey and links to North Atlantic and monsoon climate: Geology 34, p. 361–364, https://doi.org/10.1130/G22407.1.

Jones, M.D., Roberts, C.N., and Leng, M.J., 2007, Quantifying climatic change through the last glacial-interglacial transition based on lake isotope palaeohydrology from central Turkey: Quaternary Research, v. 67, p. 463–473, https://doi.org/10.1016/j.yqres.2007.01.004.

Karadenizli, L., 2011, Oligocene to Pliocene palaeogeographic evolution of the Çankırı-Çorum Basin, central Anatolia, Turkey: Sedimentary Geology, v. 237, p. 1–29, https://doi.org/10.1016/j.sedgeo.2011.01.008.

Kaya, F., and Kaymakçı, N., 2013, Systematics and dental microwear of the late Miocene Gliridae (Rodentia, Mammalia) from Hayranlı, Anatolia: Implications for paleoecology and paleobiodiversity: Palaeontologia Electronica, v. 16, 16.3.21A, https://doi.org/10.26879/385.

Kaya, F., Bibi, F., Žliobaitė, I., Eronen, J.T., Hui, T., and Fortelius, M., 2018, The rise and fall of the Old World savannah fauna and the origins of the African savannah biome: Nature Ecology & Evolution, v. 2, p. 241–246, https://doi.org/10.1038/s41559-017-0414-1.

Kayseri-Özer, M.S., 2017, Cenozoic vegetation and climate change in Anatolia—A study based on the IPR-vegetation analysis: Palaeogeography, Palaeoclimatology, Palaeoecology, v. 467, p. 37–68, https://doi.org/10.1016/j.palaeo.2016.10.001.

Kröner, A., and Şengör, A.M.C., 1990, Archean and Proterozoic ancestry in late Precambrian to early Paleozoic crustal elements of southern Turkey as revealed by single-zircon dating: Geology, v. 18, p. 1186–1190, https://doi.org/10.1130/0091-7613(1990)018<1186:AAPAIL>2.3.CO;2.

Kürçer, A., and Gökten, Y.E., 2012, Paleoseismological three dimensional virtual photography method; a case study: Bağlarkayası-2010 trench, Tuz Gölü fault zone, Central Anatolia, Turkey, *in* Sharkov, E., ed., Tectonics: Recent Advances: London, InTech, p. 201–228, https://doi.org/10.5772/48194.

Leng, M.J., and Marshall, J.D., 2004, Palaeoclimate interpretation of stable isotope data from lake sediment archives: Quaternary Science Reviews, v. 23, p. 811–831, https://doi.org/10.1016/j.quascirev.2003.06.012.

Leng, M.J., Roberts, N., Reed, J.M., and Sloane, H.J., 1999, Late Quaternary palaeohydrology of the Konya Basin, Turkey, based on isotope studies of modern hydrology and lacustrine carbonates: Journal of Paleolimnology, v. 22, p. 187–204, https://doi.org/10.1023/A:1008024127346.

Le Pennec, J.-L., Bourdier, J.-L., Froger, J.-L., Temel, A., Camus, G., and Gourgaud, A., 1994, Neogene ignimbrites of the Nevsehir plateau (central Turkey): Stratigraphy, distribution and source constraints: Journal of Volcanology and Geothermal Research, v. 63, p. 59–87, https://doi.org/10.1016/0377-0273(94)90018-3.

Lepetit, P., Viereck, L., Piper, J.D.A., Sudo, M., Gürel, A., Çopuroğlu, I., Gruber, M., Mayer, B., Koch, M., Tatar, O., and Gürsoy, H., 2014, $^{40}Ar/^{39}Ar$ dating of ignimbrites and Plinian air-fall layers from Cappadocia, Central Turkey: Implications to chronostratigraphic and Eastern Mediterranean palaeoenvironmental record: Chemie der Erde–Geochemistry, v. 74, p. 471–488, https://doi.org/10.1016/j.chemer.2014.05.001.

Li, H.-C., and Ku, T.-L., 1997, $\delta^{13}C$–$\delta^{18}C$ covariance as a paleohydrological indicator for closed-basin lakes: Palaeogeography, Palaeoclimatology, Palaeoecology, v. 133, p. 69–80, https://doi.org/10.1016/S0031-0182(96)00153-8.

Lüdecke, T., Mikes, T., Rojay, F.B., Cosca, M.A., and Mulch, A., 2013, Stable isotope-based reconstruction of Oligo-Miocene paleoenvironment and paleohydrology of Central Anatolian lake basins (Turkey): Turkish Journal of Earth Sciences, v. 22, p. 793–819, https://doi.org/10.3906/yer-1207-11.

Mazzini, I., Hudáčková, N., Joniak, P., Kováčová, M., Mikes, T., Mulch, A., Rojay, F.B., Lucifora, S., Esu, D., and Soulié-Märsche, I., 2013, Palaeoenvironmental and chronological constraints on the Tuğlu Formation (Çankırı Basin, Central Anatolia, Turkey): Turkish Journal of Earth Sciences, v. 22, p. 747–777, https://doi.org/10.3906/yer-1207-10.

McKenzie, D., 1976, The East Anatolian Fault: A major structure in eastern Turkey: Earth and Planetary Science Letters, v. 29, p. 189–193, https://doi.org/10.1016/0012-821X(76)90038-8.

Meijers, M.J.M., Strauss, B.E., Özkaptan, M., Feinberg, J.M., Mulch, A., Whitney, D.L., and Kaymakçı, N., 2016, Age and paleoenvironmental reconstruction of partially remagnetized lacustrine sedimentary rocks (Oligocene Aktoprak basin, central Anatolia, Turkey): Geochemistry Geophysics Geosystems, v. 17, p. 914–939, https://doi.org/10.1002/2015GC006209.

Meijers, M.J.M., Peynircioğlu, A.A., Cosca, M.A., Brocard, G.Y., Whitney, D.L., Langereis, C.G., and Mulch, A., 2018a, Climate stability in Central Anatolia during the Messinian Salinity Crisis: Palaeogeography, Palaeoclimatology, Palaeoecology, v. 498, p. 53–67, https://doi.org/10.1016/j.palaeo.2018.03.001.

Meijers, M.J.M., Brocard, G.Y., Cosca, M.A., Lüdecke, T., Teyssier, C., Whitney, D.L., and Mulch, A., 2018b, Rapid late Miocene surface uplift of the Central Anatolian Plateau margin: Earth and Planetary Science Letters, v. 497, p. 29–41, https://doi.org/10.1016/j.epsl.2018.05.040.

Monod, O., 1977, Recherches géologiques dans le Taurus Occidental au sud de Beyflehir (Turquie) [Ph.D. thesis]: Paris, Université Paris-Sud Orsay, 442 p.

MTA (General Directorate of Mineral Research and Exploration of Turkey), 2019, 1:100,000 geological maps, http://www.mta.gov.tr/eng/maps/geological-100000.

Ocakoğlu, F., 2002, Palaeoenvironmental analysis of a Miocene basin in the high Taurus Mountains (southern Turkey) and its palaeogeographical and structural significance: Geological Magazine, v. 139, p. 473–487, https://doi.org/10.1017/S0016756802006544.

Ocakoğlu, F., 2004, Mio-Pliocene basin development in the eastern part of the Cappadocian Volcanic Province (Central Anatolia, Turkey) and its implications for regional tectonics: International Journal of Earth Sciences, v. 93, p. 314–328, https://doi.org/10.1007/s00531-004-0390-y.

Öğretmen, N., Cipollari, P., Frezza, V., Faranda, C., Karanika, K., Gliozzi, E., Radeff, G., and Cosentino, D., 2018, Evidence for 1.5 km of uplift of the Central Anatolian Plateau's southern margin in the last 450 kyr and implications for its multi-phased uplift history: Tectonics, v. 37, p. 359–390, https://doi.org/10.1002/2017TC004805.

Okay, A.I., and Tüysüz, O., 1999, Tethyan sutures of northern Turkey, *in* Durand, B., Jolivet, L., Horváth, F., and Séranne, M., eds., The Mediterranean Basins: Tertiary Extension within the Alpine Orogen: Geological Society of London Special Publication 156, p. 475–515, https://doi.org/10.1144/GSL.SP.1999.156.01.22.

Önal, M., Helvaci, C., and Ceyhan, F., 2004, Geology and trona potential of the Middle Miocene Gürün (Sivas) Basin, Central Anatolia, Turkey: Carbonates and Evaporites, v. 19, p. 118–132, https://doi.org/10.1007/BF03178475.

Özgül, N., 1984, Stratigraphy and tectonic evolution of the Central Taurides, *in* Tekeli, O., and Göncüoğlü, M.C., eds., Geology of the Taurus Belt: International Symposium, Mineral Research and Exploration Institute, Ankara, 26–29 September 1983: Ankara, Geological Society of Turkey and the Mineral Research and Exploration Institute, p. 77–90.

Özsayin, E., Çiner, A., Rojay, B., Dirik, K., Melnick, D., Fernández-Blanco, D., Bertotti, G., Schildgen, T.F., Garcin, Y., Strecker, M.R., and Sudo, M., 2013, Plio-Quaternary extensional tectonics of the Central Anatolian Plateau: A case study from the Tuz Gölü Basin, Turkey: Turkish Journal of Earth Sciences, v. 22, p. 691–714, https://doi.org/10.3906/yer-1210-5.

Piper, J.D.A., Koçbulut, F., Gürsoy, H., Tatar, O., Viereck, L., Lepetit, P., Roberts, A.P., and Akpınar, Z., 2013, Palaeomagnetism of the Cappadocian Volcanic Succession, Central Turkey: Major ignimbrite emplacement during two short (Miocene) episodes and Neogene tectonics of the Anatolian collage: Journal of Volcanology and Geothermal Research, v. 262, p. 47–67, https://doi.org/10.1016/j.jvolgeores.2013.06.008.

Poisson, A., Vrielynck, B., Wernli, R., Negri, A., Bassetti, M.-A., Büyükmeriç, Y., Özer, S., Guillou, H., Kavak, K.S., Temiz, H., and Orszag-Sperber, F., 2016, Miocene transgression in the central and eastern parts of the Sivas Basin (Central Anatolia, Turkey) and the Cenozoic palaeogeographical evolution: International Journal of Earth Sciences, v. 105, p. 339–368, https://doi.org/10.1007/s00531-015-1248-1.

Radeff, G., Schildgen, T.F., Cosentino, D., Strecker, M.R., Cipollari, P., Darbaş, G., and Gürbüz, K., 2017, Sedimentary evidence for late Messinian uplift of the SE margin of the Central Anatolian Plateau: Adana Basin, southern Turkey: Basin Research, v. 29, p. 488–514, https://doi.org/10.1111/bre.12159.

Radwany, M., Whitney, D.L., Brocard, G., Umhoefer, P.J., and Teyssier, C., 2017, Ophiolite gabbro from source to sink: A record of tectonic and surface processes in Central Anatolia: Geosphere, v. 13, p. 1329–1358, https://doi.org/10.1130/GES01465.1.

Roberts, N., Reed, J.M., Leng, M.J., Kuzucuoğlu, C., Fontugne, M., Bertaux, J., Woldring, H., Bottema, S., Black, S., Hunt, E., and Karabiyikoğlu, M., 2001, The tempo of Holocene climatic change in the eastern Mediterranean region: New high-resolution crater-lake sediment data from central Turkey: The Holocene, v. 11, p. 721–736, https://doi.org/10.1191/09596830195744.

Rojay, B., and Karaca, A., 2008, Post-Miocene deformation in the south of the Galatean Volcanic Province, NW of Central Anatolia (Turkey): Turkish Journal of Earth Sciences, v. 17, p. 653–672.

Schemmel, F., Mikes, T., Rojay, B., and Mulch, A., 2013, The impact of topography on isotopes in precipitation across the Central Anatolian Plateau (Turkey): American Journal of Science, v. 313, p. 61–80, https://doi.org/10.2475/02.2013.01.

Schleiffarth, W.K., Darin, M.H., Reid, M.R., and Umhoefer, P.J., 2018, Dynamics of episodic Late Cretaceous–Cenozoic magmatism across Central to Eastern Anatolia: New insights from an extensive geochronology compilation: Geosphere, v. 14, p. 1990–2008, https://doi.org/10.1130/GES01647.1.

Şengör, A.M.C., Tüysüz, O., Imren, C., Sakınç, M., Eyidoğan, H., Görür, N., Le Pichon, X., and Rangin, C., 2005, The North Anatolian fault: A new look: Annual Review of Earth and Planetary Sciences, v. 33, p. 37–112, https://doi.org/10.1146/annurev.earth.32.101802.120415.

Shi, X., Pu, T., He, Y., Qi, C., Zhang, G., and Xia, D., 2017, Variability of stable isotope in lake water and its hydrological processes identification in Mt. Yulong region: Water, v. 9, 711, https://doi.org/10.3390/w9090711.

Sobel, E.R., Hilley, G.E., and Strecker, M.R., 2003, Formation of internally drained contractional basins by aridity-limited bedrock incision: Journal of Geophysical Research, v. 108, 2344, https://doi.org/10.1029/2002JB001883.

Spötl, C., and Vennemann, T.W., 2003, Continuous-flow isotope ratio mass spectroscopic analysis of carbon minerals: Rapid Communications in Mass Spectrometry, v. 17, p. 1004–1006, https://doi.org/https://doi.org/10.1002/rcm.1010.

Strecker, M.R., Alonso, R.N., Bookhagen, B., Carrapa, B., Hilley, G.E., Sobel, E.R., and Trauth, M.H., 2007, Tectonics and

climate of the southern central Andes: Annual Review of Earth and Planetary Sciences, v. 35, p. 747–787, https://doi.org/10.1146/annurev.earth.35.031306.140158.

Strömberg, C.A.E., Werdelin, L., Friis, E.M., and Saraç, G., 2007, The spread of grass-dominant habitats in Turkey and surrounding areas during the Cenozoic: Phytolith evidence: Palaeogeography, Palaeoclimatology, Palaeoecology, v. 250, p. 18–49, https://doi.org/10.1016/j.palaeo.2007.02.012.

The NOW Community, 2017, New and Old Worlds Database of Fossil Mammals (NOW). Licensed under CC BY 4.0. Release [number of release], retrieved January 2017 from http://www.helsinki.fi/science/now/ (last accessed January 2017).

Üstün, A., Tuşat, E., Yalvaç, S., Özkan, İ., Eren, Y., Özdemir, A., Bildirici, İ.Ö., Üstüntaş, T., Kırtıloğlu, O.S., Mesutoğlu, M., Doğanalp, S., Canaslan, F., Abbak, R.A., Avşar, N.B., and Şimşek, F.F., 2015, Land subsidence in Konya Closed Basin and its spatio-temporal detection by GPS and DInSAR: Environmental Earth Sciences, v. 73, p. 6691–6703, https://doi.org/10.1007/s12665-014-3890-5.

Wen, R., Tian, L., Liu, F., and Qu, D., 2016, Lake water isotope variation linked with the in-lake water cycle of the alpine Bangong Co, arid western Tibetan Plateau: Arctic, Antarctic, and Alpine Research, v. 48, p. 563–580, https://doi.org/10.1657/AAAR0015-028.

Whitney, D.L., and Hamilton, M.A., 2004, Timing of high-grade metamorphism in central Turkey and the assembly of Anatolia: Journal of the Geological Society, v. 161, p. 823–828, https://doi.org/10.1144/0016-764903-081.

Wilson, M., Tankut, A., and Guleç, N., 1997, Tertiary volcanism of the Galatia province, north-west Central Anatolia, Turkey: Lithos, v. 42, p. 105–121, https://doi.org/10.1016/S0024-4937(97)00039-X.

Yavuz, N., Culha, G., Demirer, Ş.S., Utescher, T., and Aydın, A., 2017, Pollen, ostracod and stable isotope records of palaeoenvironment and climate: Upper Miocene and Pliocene of the Çankırı Basin (Central Anatolia, Turkey): Palaeogeography, Palaeoclimatology, Palaeoecology, v. 467, p. 149–165, https://doi.org/10.1016/j.palaeo.2016.04.023.

Yıldırım, C., 2014, Relative tectonic activity assessment of the Tuz Gölü fault zone; Central Anatolia, Turkey: Tectonophysics, v. 630, p. 183–192, https://doi.org/10.1016/j.tecto.2014.05.023.

Yıldırım, C., Schildgen, T.F., Echtler, H., Melnick, D., and Strecker, M.R., 2011, Late Neogene and active orogenic uplift in the Central Pontides associated with the North Anatolian Fault: Implications for the northern margin of the Central Anatolian Plateau, Turkey: Tectonics, v. 30, TC5005, https://doi.org/10.1029/2010TC002756.